HHS Public Access
Author manuscript
ACS Nano. Author manuscript; available in PMC 2023 March 07.

Modulating Nanoparticle Size to Understand Factors Affecting Hemostatic Efficacy and Maximize Survival in a Lethal Inferior Vena Cava Injury Model

Celestine Hong[†,⌐], **Osaid Alser**[§], **Anthony Gebran**[§], **Yanpu He**[†], **Wontae Joo**[†,⌐], **Nikolaos Kokoroskos**[§], **George Velmahos**[*,§], **Bradley D. Olsen**[*,†,⌐], **Paula T. Hammond**[*,†,⌐]

[†]Department of Chemical Engineering, Massachusetts Institute of Technology, Cambridge, MA 02139, USA

[⌐]Institute for Soldier Nanotechnologies, Massachusetts Institute of Technology, Cambridge, Massachusetts 02139, USA

[§]Division of Trauma, Emergency Surgery and Surgical Critical Care, Department of Surgery, Massachusetts General Hospital & Harvard Medical School, Boston, Massachusetts 02144, USA

Abstract

Intravenous nanoparticle hemostats offer a potentially attractive approach to promote hemostasis, in particular for inaccessible wounds such as non-compressible torso hemorrhage (NCTH). In this work, particle size was tuned over a range of <100 nm – 500 nm, and its effect on nanoparticle-platelet interactions was systematically assessed using *in vitro* and *in vivo* experiments. Smaller particles bound a larger percentage of platelets per mass of particle delivered, while larger particles resulted in higher particle accumulation on a surface of platelets and collagen. Intermediate particles led to the greatest platelet content in platelet-nanoparticle aggregates, indicating that they may be able to recruit more platelets to the wound.

In biodistribution studies, smaller and intermediate nanoparticles exhibited longer circulation lifetimes, while larger nanoparticles resulted in higher pulmonary accumulation. The particles were then challenged in a two-hour lethal inferior vena cava (IVC) puncture model, where intermediate nanoparticles significantly increased both survival and injury-specific targeting relative to saline and unfunctionalized particle controls. An increase in survival in the second

hour was likewise observed in the smaller nanoparticles relative to saline controls, though no significant increase in survival was observed in the larger nanoparticle size. In conjunction with prior *in vitro* and *in vivo* experiments, these results suggest that platelet content in aggregates and extended nanoparticle circulation lifetimes are instrumental to enhancing hemostasis. Ultimately, this study elucidates the role of particle size in platelet-particle interactions, which can be a useful tool for engineering the performance of particulate hemostats and improving the design of these materials.

Graphical Abstract
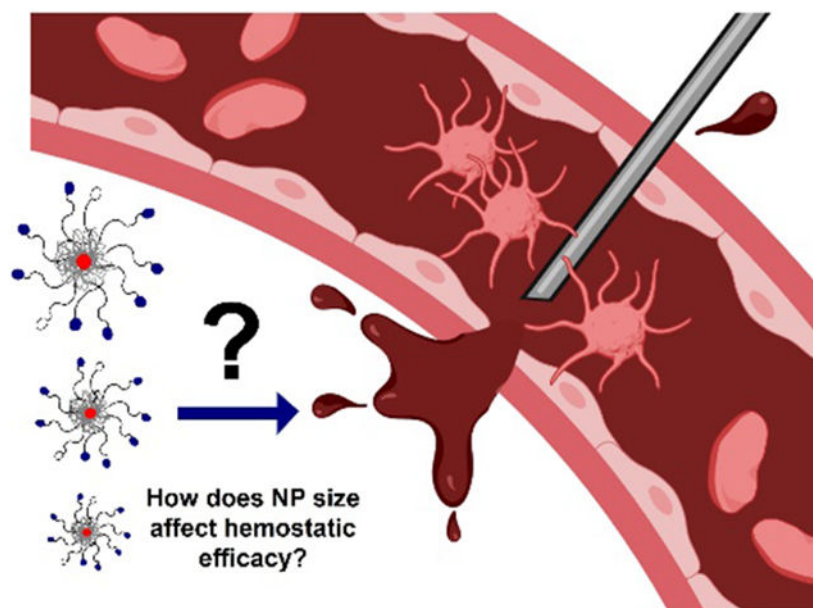
Keywords

hemostasis; internal injury; nanoparticle; platelet; particle size; non-compressible hemorrhage

---

INTRODUCTION

Hemorrhage following trauma represents the leading cause of death in the US population below age 46 and accounts for over 1.5 million deaths per year worldwide[1]. Of these casualties, up 80 percent are considered potentially preventable, with the majority stemming from non-compressible bleeding in the torso (NCTH) [2-5]. In particular, closed wounds with internal bleeding are difficult to identify and treat without invasive techniques[6] or advanced imaging modalities[7, 8], as their assessment is limited to inferences based on changes in vital signs[9].

To address this need, researchers in the field have sought to develop intravenously-administered materials that target the injury site through interaction with wound-specific cells or proteins, and have succeeded in validating their performance over a wide variety of injury models. These include polymers with fibrin-crosslinking sidechains[10], liposomal

formulations with adhesive moieties that bind to von Willebrand factor[11], and albumin microparticles functionalized with a fibrinogen-derived dodecapeptide (H12)[12]. Polymeric nanoparticles (NPs) functionalized with platelet-aggregating peptides – such as GRGDS -PEG-PLGA – have likewise demonstrated significantly increased survival in blunt trauma, blast trauma, and femoral artery injury models[13-15]. Furthermore, they have been directly shown to withstand harsh storage conditions, which is a critical factor for eventual field deployment [16]. Though challenges such as off-target effects[6] and infusion reactions remain [17], polymeric nanoparticle hemostats present a promising solution to treating internal hemorrhage in a prehospital setting.

The safe and effective systemic administration of hemostatic nanoparticles is heavily dependent on the particle's biodistribution and concentration in the bloodstream, its ability to target and interact selectively with wound components, and its ability to circulate in the bloodstream long enough to accumulate at the site of vascular injury[18] without inducing off-target effects. Due to the design of these materials to amplify hemostatic responses, it is imperative that they are able to specifically target the wound site to avoid the initiation of procoagulant behavior elsewhere. In fact, increased occurrence of microthrombi in the lungs has been reported with the use of hemostatic nanoparticles as a potential side effect of off-target lung accumulation[19], and higher concentrations of both liposomal and polymeric formulations have also been shown to cause cardiopulmonary distress [14, 19].

Particle size has long been known to be a crucial factor in the targeting ability, circulation lifetime, and biodistribution of therapeutics[20]. Nanoparticles larger than 150 nm have been reported to result in increased pulmonary and splenic accumulation, whereas those smaller than 5 nm can be rapidly subject to renal clearance [21]. Multiple studies in the cancer literature have leveraged this phenomenon by tuning the size and other surface characteristics of nanoparticles in order to achieve higher blood circulation lifetimes and tumor accumulation[22-24]. While a significant number of studies have focused on the treatment of cancer, the importance of particle size has likewise been investigated in other fields for its targeting and circulation properties, from traversing the blood-brain barrier to treating disorders in the central nervous system[25] to using particles as imaging agents for microvascular blood flow[26].

However, research on the effect of particle size in enhancing the performance of particle-based hemostats has been relatively limited. For intravenous hemostats, studies have only been performed with sizes an order of magnitude apart (200 nm *vs.* micron-sized liposomes) [19]; for systemic polymeric systems, it remains an unexplored area of interest. The sizes of hemostatic polymer particles studied in literature range from approximately 400 to 600 nm, a size cutoff known to not only favor retention in the spleen[21], but also result in decreased circulation lifetimes[24]. As briefly noted earlier, the particles have also been demonstrated to accumulate in the lungs even for control, non-hemostatic particles[13], and have shown high accumulation of activated platelet-targeting nanoparticles in the lungs for a traumatic liver injury[6, 27]. This could be a cause for concern, considering that the lung is a major site for platelet biogenesis, sequestration, and activity[28, 29]. Furthermore, while enhancement of platelet aggregation is well studied, the effect of particle size on other mechanisms of clotting has not been explored. Given the varied mechanisms by which these materials are

proposed to modulate hemostasis (such as targeting capability[19, 30], platelet adhesion and aggregation[6, 14, 16], particle flexibility[19], shape[19], and circulation lifetime[19]), a thorough study on how particle size affects interactions with its targets and how these effects can be leveraged to maximize therapeutic efficacy is needed.

In this work, the effect of particle size is systematically explored through fundamental studies of particle interactions with platelets or wound-mimetic surfaces *in vitro* as well as *in vivo* performance. By tuning the size of nanoparticles through various formulation techniques, a series of five sizes was generated, encompassing a range of <100 nm to 500-650 nm using a single block copolymer. These particles were tested extensively *in vitro* to gauge the influence of size on the number of activated platelets bound per unit mass of particle, the degree of platelet aggregation, and the total particle mass adhered to a wound mimetic surface. They were then assessed *in vivo* to obtain circulation lifetimes, *in vivo* biodistribution, and terminal organ biodistribution in uninjured mice. Based on these studies, small, intermediate, and large nanoparticle sizes (<100 nm, 140-220 nm, and 500-650 nm, respectively) were then selected for further testing in a double inferior vena cava (IVC) puncture injury, where both small and intermediate nanoparticles were observed to significantly increase survival relative to the saline control. Accumulation at the injury site was observed in the groups with improved survival. Overall, particle size is demonstrated to be a critical factor in determining the performance of intravenous hemostats in a major vessel hemorrhage model, and may serve as an important reference in optimizing and engineering future designs for the treatment of internal bleeding.

RESULTS AND DISCUSSION

Polymer and nanoparticle synthesis and characterization:

PEG-b-PLGA block copolymer was used to synthesize nanoparticles of sub-100 nm to > 500 nm in diameter (Figure 1). Two batches of polymer, Batch 1 and Batch 2 were synthesized with the procedure described in Figure 1a, with Batch 2 used predominantly for particle stability and large animal studies and Batch 1 for all remaining *in vitro* and *in vivo* assays unless otherwise specified. All chemical characterization of Batches 1 and 2 (NMR, GPC, peptide conjugation efficiency, and DLS) has been provided in the Supporting Information (Figures S1-S3, Table S1).

Nanoparticle synthesis was adapted from nanoprecipitation and dialysis protocols in the literature [6, 31], with ~1 mg of pure 50:50 lactide: glycolide PLGA (~31kDa) added to achieve lower particle polydispersity. As shown in Figure 1b, particle size distributions were obtained through dynamic light scattering (DLS), with five distinct populations achieved through the use of various solvents and polymer concentrations (Table 1). Sizes of 91.4 ± 1.5 nm, 120.6 ± 2.2 nm, 165.2 ± 3.7 nm, 356 ± 15 nm, and 533 ± 20 nm were achieved for the unlabeled particles. The lower bound was defined by limitations on nanoparticle synthesis and stability, whereas the upper size range of 650 nm was capped to minimize complement activation effects resulting from microparticle delivery[32-35]. Nanoparticles were found to adopt an approximately spherical morphology (TEM, negative staining) as shown in Figure S4. Their dried diameter was observed to be smaller (60-70%) in comparison to their hydrodynamic size as measured via dynamic light scattering (DLS), a phenomenon that has

been previously noted in literature[36, 37]. The size trend observed for different groups were consistent with DLS results. All particles exhibited relatively low polydispersities (PDI, $(\frac{\text{Standard Deviation}}{Mean})^2 < 0.3$), as well as a negative (-15 mV ~ -30 mV) surface zeta potential. Dye-labeled nanoparticles were formed by mixing the formulation with approximately 10 wt% of the dye-conjugated polymer (either Cyanine 7 or Cyanine 5) to the unlabeled GRGDS-PEG-b-PLGA and pure PLGA, using the same synthesis methods required to create the unlabeled nanoparticles (Figure 1c). Minimal changes in size were observed despite the introduction of the dye-functionalized polymer (Table S1). The sizes of each of the specific particles not reported here (labeled and labeled, Batch 1 and Batch 2) have been summarized in the Supporting Information (Table S1).

To validate the size stability of the nanoparticles over the timeframe of the *in vivo* experiment (2 hours), they were first incubated under agitation in cell culture media with serum at 37 °C, during which their sizes were recorded *via* DLS (Figure 2a) at set time intervals. While varying levels of size change were observed for the different particles (Figure 2b), all sizes remained within 20% of the size measured at t = 0 in serum for the first three hours. The size changes also appeared to plateau as time went on, with minimal variation observed between the third hour and three days post-incubation except for the 500-650 nm group, which continued to decrease in size significantly. This could potentially be due to its continued approach towards the 140-220 nm group, the size that appeared to be most kinetically stable. The stability of concentrated nanoparticle solutions (20 mg/mL) kept static at room temperature (20 °C) in deionized water was also measured, again by tracking the particle size change over several days *via* DLS. As can be seen in Figure 2c, these sizes were found to remain largely constant over the five-day period when the nanoparticles were stored in water.

In a follow-up experiment, the stability of the peptide bound to the nanoparticle was assessed. Nanoparticle stock solutions were formulated in platelet-rich-plasma (PRP), incubated for sixteen hours at 37 °C under agitation, and used directly in a transmission-based aggregation assay. No significant differences were observed between fresh and overnight-incubated nanoparticles in their ability to increase platelet aggregation (Figure S5), demonstrating limited degradation of the bound peptide. Finally, the stability of the conjugated dye was assessed, specifically to detect any premature release from the nanoparticles. Release of dye was minimal under conditions mimicking animal experiments (*e.g.* incubation at 37 °C under agitation for a period of 3 hours). No significant difference in fluorescence of the media could be detected between the nanoparticle groups and the pure media with no nanoparticle (Figure 2d, 2e), indicating that dye was not released from the particles.

In vitro platelet aggregation and coagulation

All functionalized nanoparticle (FP) sizes tested in sodium citrate-anticoagulated platelet-rich plasma (PRP) were able to elicit increased platelet aggregation when compared to the positive control without particle (Figure 3). A decrease in transmission in coagulation tests indicates fibrin polymerization, whereas an increase in transmission during aggregation tests indicates the formation of platelet aggregates. Results from the aggregation assay were

similar to other studies in the field, where both maximum and endpoint aggregation were observed to peak at a specific concentration before decreasing with increasing particle concentration[6]. Platelet aggregation was induced by the addition of agonist adenosine diphosphate (ADP) to PRP at a concentration of 10 μM, and up to a four-fold increase in transmission was observed upon the addition of FPs at various concentrations. All FP concentrations and sizes tested increased transmission relative to the positive control when added to PRP and ADP but did not appear to induce aggregation without an agonist. Smaller particles maximized aggregation at a lower concentration (Figure 3), regardless of the metric used to quantify aggregation (either endpoint or maximum aggregation). As identical masses of particles were added to the wells irrespective of particle size, the observed shift in optimal concentration could be due to the larger surface area/mass ratio of smaller particles, which could result in a great exposure of the targeting GRGDS residues per unit mass – and potentially a lower dosage required to achieve similar therapeutic efficacy.

Aggregation tests of polymer from Batch 2, as well as both Cy5 and Cy7-labeled nanoparticles were repeated at a set concentration of 1.5 mg/ mL, largely to confirm their efficacy in increasing platelet aggregation. Representative aggregation curves and changes in relative aggregation for all remaining nanoparticles (Batch 2, Cy5-labeled, and Cy7-labeled) are shown in Figure S6. All particles resulted in an increase in platelet aggregability. Subsequent *in vivo* tests were conducted at a particle concentration of ~1.0 mg/ mL blood, a concentration at which relative aggregation was increased by at least 50% for all particle sizes.

When compared to the smallest particle size group, it appeared that many of the larger particle sizes were able to induce a greater increase in transmission (>200% relative to the positive control). This could be indicative of increased platelet aggregation or simply due to an increase in particle size, as light scattering effects were more significant with larger particles. To supplement these results and determine the true ability of nanoparticles to aggregate onto a surface, an additional assay on lactate dehydrogenase content was conducted to quantify the platelet content in these platelet-nanoparticle aggregates (Figure 4).

A slight increase in the binding of activated platelets was observed for all nanoparticle sizes in comparison to the ADP-only positive control, with a maximum value observed at an intermediate size of 140-220 nm s(Figure 4a). This was in line with results shown in the transmission-based aggregation assay when accounting for the addition of washing steps to fully remove any aggregates in suspension, which could result in the smaller magnitude of change observed. Subtraction of nonspecific binding to quiescent platelets, which appeared to trend upwards with decreasing nanoparticle size, revealed that this amounted to a two-fold increase at 1 mg/ mL relative to the positive control. To investigate the possibility of synergistic effects between different nanoparticle sizes, an equimass mixture of small, intermediate and large nanoparticles was also prepared by combining solutions of the three sizes. Mixed nanoparticles were observed to significantly increase platelet recruitment to a surface, in between that of intermediate and large nanoparticles (Figure S7). Ultimately, the 140-220 nm size group was demonstrated to be significantly better than all other groups at specifically enhancing the formation of platelet aggregates that remained adherent after

multiple washing steps, which could be of interest considering the constant state of blood flow *in vivo*.

Finally, the hemostatic nanoparticles were tested with a transmission-based coagulation assay, in which the decrease in transmission over the course of fibrin polymerization was measured with a plate reader Coagulation was induced in citrated blood *via* the addition of calcium chloride, and the addition of hemostatic nanoparticle did not result in spontaneous coagulation for all sizes. Consistent with literature results, the 500-650 nm particle sizes resulted in decreased levels of relative coagulation for both Batch 1 and Batch 2 at concentrations where optimal aggregation was achieved; in fact, this effect was exacerbated with increasing particle concentration (Figure S8)[6]. This could be attributed to the much lower transmission values introduced by light scattering from large particles, which could not be isolated from the change in transmission from fibrin polymerization. All other particle sizes resulted in minimal change in levels of relative coagulation.

Particle binding to platelets

The size of functionalized particles was found to significantly influence their ability to specifically bind activated platelets under flow, while platelet activation and differentiation into procoagulant platelets were not affected by the addition of hemostatic nanoparticles. In brief, various agonists and agonist combinations (thrombin, ADP, and collagen) were screened with a single particle size (<100 nm) to determine the best activation conditions, dilution of PRP, and concentration range of particles. Thrombin, collagen, and thrombin + collagen combinations were found to elicit higher levels of platelet activation when compared to ADP, as determined through CD62P^{+} cells (marker for P-selectin). Thrombin was eventually selected as the agonist for all further studies, as no differences in platelet activation or production of procoagulant platelets were observed with the addition of collagen in an acetic acid solution (Figure S9). Figure 5a provides representative dot plots on the gating strategy to remove nanoparticle-only fluorescence, with additional dot plots to obtain the percentage of nanoparticle-bound platelets shown in Figure S10.

The introduction of pro-aggregatory nanoparticles does not appear to affect the percentage of platelets that undergo activation (CD62P^{+} / CD41^{+}) or differentiate into procoagulant platelets (Annexin V / CD62P^{+}), and there is some degree of nonspecific binding of the nanoparticle to quiescent platelets that trends upwards with increasing size (Figure 5b, 5c). When normalized to account for nonspecific binding, smaller particles bound a greater number of platelets (Figure 5d), which could again be due to a greater surface area/ mass ratio as noted in the previous aggregation assay.

Mixed nanoparticles again exhibited binding behavior between that of intermediate and large nanoparticles to single platelets under flow (Figure S11). This phenomenon could be observed across the concentration range tested (0.1 −2 mg nanoparticle in PRP). Data from all other concentrations tested exhibit the same trends shown in Figure 5c-d and have been provided in the Supporting Information (Figure S12). These results indicate that the specific targeting of single activated platelets under flow can likely be optimized by decreasing nanoparticle size.

Following the results of the previous study, the binding of particles to a surface was investigated, as it was possible that the few but sizeable platelet aggregates formed with larger particles could settle to the bottom of a tube or be filtered out, and hence be more difficult to measure under flow. Additionally, this assay sought to elucidate any differences in the mass of functionalized polymer that could be bound on platelets on a surface, as the flow cytometry studies were only able to provide the percentages of particle-bound platelets, with little information about particle mass accumulated. Particle binding to platelets on a surface was found to significantly increase with particle size when normalized to nonspecific binding on quiescent platelets or on collagen surfaces, a trend that was visible in both concentrations tested (2 mg/ mL and 1 mg/ mL nanoparticle in PRP, Figure 6). Other concentrations (0.5 and 0.1 mg FP/ mL) tested in a pilot study of the <100 nm and 500-650 nm size group were found to be inconclusive, in part due to the large variation present in this assay. Therefore, these trial levels were discontinued before the full-scale experiment was conducted. Mixed nanoparticles exhibited behavior similar to large nanoparticles in specific binding to a platelet surface, significantly greater than nanoparticle binding from small nanoparticles (Figure S11). A schematic of the procedure is provided in Figure 6a.

Though both the number of activated platelets specifically bound under flow by hemostatic nanoparticle and the total mass of hemostatic nanoparticle accumulated on a wound-mimetic platelet surface may be used to indicate targeting of activated platelets, they follow nearly opposite trends in size. The mass of particles bound on a surface was largest with the 500-650 nm group and smallest with the <100 nm size group when normalized to the negative controls (Figure 6b, c), with larger particles resulting in the formation of sizeable platelet-particle aggregates that were visible to the naked eye (representative image in clear well plates provided in Figure S13).

A potential explanation for this trend may be linked to the size of each particle relative to platelets, which are normally 2-3μm in size, with procoagulant platelets/platelet microparticles forming a separate sub-1.0 micron population. While larger nanoparticles are closer to the size scale of regular platelets and are similar in size to platelet microparticles, the <100 nm population is a full order of magnitude smaller and may lack the ability to significantly influence platelet sedimentation even when bound (the volume of each particle being ~125 times smaller than the >500 nm group). The enhanced binding of particle mass with increased size is consistent with trends reported in the microfluidics literature, where the number of bound particles decrease with increasing diameter but the total volume increases with diameter[1.3 40, 41]. Moreover, as shown in the flow cytometry studies, smaller particles were able to bind a larger number of platelets under flow and could have been removed during the multiple washing steps. Ultimately, the mass of particles bound depends on both the total mass adhered per binding event—which increases with particle size--and the total number of platelets bound per unit mass (which under flow decreases with size). As such, most comparisons could only be made between the two extremes of particle sizes. Key results from these *in vitro* assays have been summarized below in Scheme 1, underscoring the importance of comparing the results of multiple *in vitro* assays to *in vivo* performance as a means to select a suitable screening metric.

The effect of functionalized nanoparticles on coagulation factors

To ensure that nanoparticles did not impede normal function of the coagulation cascade, the effect of functionalized nanoparticles on the coagulation cascade was evaluated in the intrinsic, extrinsic, and common pathways. Intermediate sized nanoparticles were found to significantly increase the concentration of certain coagulation factors in the contact activation and common coagulation pathways (Figure S14). Specifically, the incubation of intermediate and mixed particles in platelet-rich-plasma at a concentration of 1 mg/ mL resulted in a significantly higher level of FIXa relative to particle-free controls at 30 minutes post-incubation. Intermediate and large nanoparticles also resulted in a significantly higher level of thrombin 5 minutes post-incubation. This may be associated with increased contact activation from platelet recruitment, as the phosphatidylserine on activated platelets provide a negatively-charged surface, which could result in higher concentrations of FXIIa and FXIa in serum that could in turn activate FIXa. However, the effect on thrombin generation appears to be short-lived, as evidenced by the decrease in thrombin concentration back to baseline at 20 minutes post-incubation. This may be due to the separation of platelets from platelet-rich-plasma (platelet-free-plasma is required to conduct these assays), which provide critical sites for the conversion of prothrombin to thrombin. Ultimately, the inclusion of various nanoparticle sizes has been shown to either to increase or not affect the concentration of coagulation factors in the intrinsic, extrinsic, and common pathways, but not detract from normal coagulation factor activity.

Organ biodistribution, retention, and blood circulation lifetime of functionalized nanoparticles in an uninjured mouse model

In order to select trial conditions for a murine lethal injury model, nanoparticles were first injected into uninjured mice to assess their circulation lifetimes and organ distributions. The mice were imaged live using IVIS for a duration of three hours and observed for several days thereafter to ensure no deleterious side effects following the injection (Figure 7a shows the timeline for blood sampling and imaging post-injection). When injected to achieve an estimated final therapeutic concentration of approximately 1 mg/ mL in mouse blood, particles of different sizes were found to have different retention times and organ accumulation (Figure 7b, 7c), specifically increased splenic accumulation in the larger particle sizes *vs.* predominantly liver accumulation in the < 100 nm size group.

Particles of all sizes accumulated for the most part in the spleen and liver, which was consistent with literature results on similar particles, in contrast to free dye that was quickly transported to the gastrointestinal and renal system and excreted (Figure 7c). Certain sizes also appeared to have greater retention times—evaluated as fluorescence over the entire animal—than others when comparing images taken at the 2h and 3h timepoints, for example when comparing the 120 nm or 180 nm (small-intermediate) particle sizes with the 325 and 575 nm (larger) sizes.

The aforementioned observations regarding organ accumulation and retention time were all confirmed by quantitative data in Figure 8 and IVIS images. Figures 8a and 8b provide the biodistribution of each particle size group (fluorescence and fluorescence per unit organ mass, respectively), with the total radiant efficiency of each organ normalized to the total

radiant efficiency over all organs from that particular animal. Due to differences in food intake and generally low particle accumulation per unit mass, the gastrointestinal (GI) system was not included in the analysis for organ biodistribution, though representative images of the free dye control (excreted through the GI tract) have been provided in Figure S15. As can be seen, the particles predominantly accumulate in the spleen and liver as previously observed from IVIS images, with an obvious trend in lung accumulation appearing when organ mass was accounted for. Specifically, highly significant differences (p 0.001) between size groups could now be observed, with smaller particles accumulating in larger amounts in the liver and in smaller quantities in the lungs and spleen when compared to the 500-650 nm group.

Across all sizes tested, there appears to be an obvious trend upwards in pulmonary accumulation as nanoparticle size increases, which may be crucial to designing safer hemostats due to the reported observations in literature of hemostatic particle accumulation in lungs and increased microthrombi occurrence relative to saline controls. These biodistribution trends are in line with those observed in different fields, also with polymeric nanoparticles[21, 31, 43]. As expected, the free dye control was found to have much higher renal accumulation than nanoparticles due to its small size, and there appeared to be a trend in decreasing particle accumulation in the kidneys with increasing size (Figure 8b).

The blood circulation profiles of GRGDS-functionalized NPs were likewise influenced by particle size (Figure 8c). Smaller particles were able to remain at relatively high concentrations in the bloodstream over the course of three hours (~70% the original injected dose), while larger nanoparticles were cleared comparatively faster. In particular, the 500 nm size group dropped to approximately 50% of their original concentration in the blood at t = 0 within 30 minutes of injection, and continued to decrease until it had reached a concentration of approximately 30% by the experimental endpoint (180 minutes). These results were consistent with observations previously reported, where larger particles experienced faster clearance from the bloodstream[44]. Finally, total retention of the particles inside each mouse at t = 180 min was evaluated by taking the total radiant efficiency over the entire mouse at the experimental endpoint and normalizing it to the value measured at t = 0 (Figure 8d). This procedure was repeated with all mice, including the ones from which blood had been sampled. As expected, the small and intermediate nanoparticle size groups tested resulted in higher levels of retention when compared to the larger size groups, and when compared to the concentration of fluorescent nanoparticles in blood (Figure 8c) there appeared to be significant sequestration of particle/free dye into organs out of the bloodstream.

On the basis of these results (four *in vitro* and one *in vivo*), three nanoparticle size groups were selected for testing in an *in vivo* injury model in rats. Specifically, the small (<100 nm) size group was shown in the flow cytometry study to bind the greatest number of platelets and in the transmission-based aggregation assay to achieve optimal aggregation at the lowest concentration (1.0 mg nanoparticle / mL). They also displayed the highest accumulation in the liver. The next trial selected—the intermediate (140-220 nm) size group—was shown to be most successful at aggregating platelets onto a surface and achieved intermediate performance in other binding assays. Both these sizes also remained at higher concentrations

in the bloodstream post-injection and had lower lung accumulation than larger particle sizes. Finally, the large (500-650 nm) size group was chosen as it resulted in the maximum amount of particle mass bound to activated platelets; in addition to that, it was the closest in size to previously tested formulations (400-500 nm and ~600 nm) that had previously been shown to enhance survival in lethal injury models[6, 27]. The physiological concentration selected for further testing was approximately 1.0 mg/ mL, which corresponded to the minimum dosage at which differences between each trial and the relevant controls could be observed in all assays.

Hemostatic efficacy of various-sized GRGDS nanoparticles in a rat inferior vena cava injury model

Small, intermediate, and large hemostatic nanoparticles, along with unfunctionalized nanoparticle and saline controls were introduced to a lethal IVC puncture model (Figure 9a-c). The model was selected due to its relatively independent location from size-mediated organ clearance, as *in vivo* experiments in the preceding section have shown a tendency for smaller nanoparticles to accumulate in the liver and for larger ones to accumulate in the lungs. This could potentially conflate size-dependent organ accumulation with specific targeting, and confound nanoparticle-platelet interactions with boundary effects from smaller vessels. Moreover, lethal injury models in the nanoparticle hemostat field have predominantly focused on solid organ injury, even though major vessel injury accounts for up to 68% of non-compressible torso hemorrhage, is associated with a high mortality rate (43%)[5], and may lead to significant side effects following partial vessel occlusion[45]. Selection of a vessel nearly five thousand times larger than the largest nanoparticle size addresses these considerations, while allowing for the exclusive study of more relevant nanoparticle-platelet interactions (rat and human platelets average 2[46] and 2.5[47] microns in size, respectively). This model achieves a 73.3% mortality rate of the saline control over the course of two hours, in comparison to a lethal liver trauma model with a 55% mortality rate over the course of three hours [6].

Intermediate nanoparticles (dye-labeled included) were found to achieve a survival rate three times higher than the saline control (84.6% *vs* 26.7 %, Figure 9b). This increase in survival was significant *via* Kaplan-Meier analysis, both over the course of the two-hour experiment (P = 0.0060) and exclusively in the second hour (P = 0.0015). Intermediate nanoparticles also significantly increased survival relative to the unfunctionalized nanoparticle control (also between 140-220 nm), as well as the large nanoparticles between Hour 1 and 2. Small nanoparticles resulted in an increase in survival (69.5%) in the second hour of the experiment (P = 0.0209) with respect to the saline control. No significant improvement in survival was found for larger nanoparticles in this injury model. Though this may appear counterintuitive in light of previous successes with nanoparticles of this size range, it is important to note that these prior studies were conducted on solid organ injury models, many of which exhibit significantly lower mortality rates in the saline controls compared to the IVC puncture model[6, 13], even with similar blood loss. This is suspected to be due to the extremely high rate of blood loss in a major vessel injury; pilot studies with gauze removed at five-minute intervals to track blood loss revealed that 90.7% of the total blood loss occurred within the first five minutes post-injury (Figure S16), though this experiment was

not replicated in the full-scale study to avoid manually disrupting the clots. The full results of Kaplan-Meier analysis between different size groups and controls have been provided in Table 2, and the average survival time and mortality rates can be found in the Supporting Information (Table S2). No significant differences in blood loss were observed, though the small and intermediate size groups had lower average blood loss percentages relative to the remaining three groups (Figure 9d). This is consistent with results reported in literature for these types of lethal, uncontrolled hemorrhage models, where blood loss and survival times span a wide range of values [6, 16, 48].

Accumulation of the targeting nanoparticles at the wound site was confirmed through the use of Cy7-labeled nanoparticles. As can be seen in Figure 10a, significant difference between the injured IVC (IVC-i) and the femoral vein (FV) on the opposite leg of the cannulation site was observed in the small nanoparticle size group. The intermediate nanoparticle size group (Figure 10b) likewise resulted in significantly greater accumulation at the injured IVC relative to the FV, as well as the uninjured IVC proximal to the wound (IVC-p). Notably, this difference remained significant even when statistical analysis was conducted on all solid organs (Figure S17), as opposed to only the vessel segments shown in Figure 11.

A similar trend could be observed in the large nanoparticle size group (Figure 10c), though this difference was not significant, possibly due to the low number of labeled trials per group (n = 3). Higher lung accumulation was also observed in this size group (Figure S17c), which could also contribute to decreased accumulation at the injured IVC in comparison to the intermediate nanoparticle size. No discernible difference or trend between vessel segments could be observed in the unfunctionalized group, conceivably because those particles possessed no wound-targeting ability (Figure 11d). The average weights of all organs and vessel segments are reported in the Supporting Information (Table S3).

The aforementioned results suggest that platelet recruitment – the metric for which the intermediate size resulted in the best performance – may be most indicative of success in this injury model, in comparison to the percentage of activated platelets bound under flow and to the total mass accumulation of nanoparticle at the wound site. While smaller nanoparticles result in more specific binding events under flow, the ultimate goal is to target a surface – the injury site. Moreover, the same mass of hemostatic nanoparticle was administered to each rat, regardless of nanoparticle size, and it is possible that the optimum aggregation concentration noted in light-transmission based aggregation assays (Figure 3) contributed to the slight difference between the smaller and intermediate size groups. Circulation lifetime may likewise be a key metric in the performance of these hemostats: in the uninjured mouse model, the concentration of the large nanoparticles decreased by half within the first hour of the experiment, and continued to decrease over the course of the next hour to around 33.5%. In contrast, the small and intermediate particles decreased to 61.6% and 71.1% of their initial concentration, respectively. This may in turn affect the wound-targeting capabilities of the nanoparticles, as longer-circulating nanoparticles will possess more opportunities to interact with the injury site prior to its clearance; in fact, the normalized fluorescence per tissue mass at the injured IVC also follows the trend of intermediate > small > large. Ultimately, these results corroborate the difference in mortality observed between trials

(69.5% and 84.6% *vs* 46.2%), affirming the major effect of particle size in the treatment of a lethal IVC injury model.

CONCLUSIONS

While polymeric nanoparticles for the treatment of internal bleeding have been studied extensively over the past decade, the effect of size on material-target interactions remains unknown, and a limited number of assays exist to quantify such interactions. In this manuscript, the systematic evaluation of a well-defined nanoparticle size range with several assays revealed seemingly disparate indicators for optimum performance. Specifically, small particles resulted in a greater number of platelet binding events under flow, while large particles exhibited higher nanoparticle mass accumulation on a surface and intermediate particles led to the greatest degree of platelet adhesion. Live imaging of the nanoparticles in an uninjured model and subsequent dissection for organ biodistribution confirmed the larger particles' propensity for pulmonary accumulation despite their shorter circulation times, emphasizing the need for a safer alternative that could still achieve the desired performance *in vivo*. Finally, when challenged in an IVC puncture model, intermediate nanoparticles resulted in the most significant increase in survival overall, followed by small nanoparticles and large nanoparticles (84.6%, 69.2%, and 46.2%, respectively, in comparison to the 26.7% in saline controls). These results were corroborated by significantly greater accumulation of the small and intermediate nanoparticles at the injured IVC relative to uninjured vessel segments. Though large nanoparticles did not result in a significant increase in survival for this injury model, it likewise exhibited a visible accumulation trend at the injured IVC, demonstrating its targeting ability.

Overall, this study elucidates the effect of size on the interactions between platelets and GRGDS-functionalized nanoparticles. Additionally, it suggests that the degree of platelet adhesion is critical to improving survival in a rapid exsanguination model like the IVC puncture model, which could be of use in the screening of other hemostatic materials for similar injuries. The aforementioned findings provide evidence of significant size-mediated effects in the treatment of major hemorrhage, marking it as an important consideration in the conception of future intravenous hemostats and potentially informing the design of other targeting agents based on their desired effects.

METHODS / EXPERIMENTAL

Materials

All chemicals and proteins were purchased from Sigma Aldrich unless otherwise specified. GRGDS peptide (95%) was purchased from China Peptides. GPRP-NH$_2$ peptide was purchased from Bachem. AF488 anti-human CD41 antibody, BV421 anti-human CD62P antibody, and PE Annexin V were purchased from BioLegend Inc. RIPA lysis and extraction buffer, Pierce 660 Protein Assay Reagent and α–MEM cell culture media were purchased from Thermo Fisher Scientific. Cyanine 7 free acid (Cy7) and Cyanine 5 free acid (Cy5) were purchased from Lumiprobe. Paraformaldehyde 4% was purchased from VWR. Deuterated solvents (CDCl$_3$ and DMSO-d$_6$) were purchased from Cambridge Isotope Laboratories. Citrated whole human blood was acquired from Research Blood Components

(Watertown, MA). Female BALB/c mice were purchased from Taconic. Sprague-Dawley rats (450-600 g) were purchased from Charles River Laboratories.

Characterization Methods

^{1}H NMR spectroscopy (400 MHz) was carried out on a Bruker Advance III DPX 400 spectrometer in deuterated DMSO at a concentration of 5 mg/ mL.(Batch 1 with 0.05 wt% TMS as an internal standard). Lactide protons (~5.20 ppm) and glycolide protons (~4.80 ppm) were used to quantify the ratio of lactide: glycolide (55:45-60:40), and the exact molecular weight of the polymer was computed from the known molecular weight of either OH-PEG-NH$_2$ or mPEG-OH (5 kDa) relative to the integration of the PEG peak at (~3.50 ppm). MestReNova softare was used to perform the analysis.

Gel permeation chromatography (GPC) was performed using an Agilent 1260 GPC system with three DMF ResiPore columns, a Wyatt Mini-DAWN TREOS 3-angle static light scattering detector, and a Wyatt Optilab T-rEX refractive index detector, with DMF + 0.01M LiBr used as the eluent.

Amino acid analysis was performed to determine the peptide conjugation efficiency of the polymers. In brief, ~10 mg of polymer was dissolved in 1 mL of 6N HCl and hydrolyzed for a day at 105 °C. Following that, HCl was removed *via* vacuum, and the residue re-dissolved in 0.1 N HCl for analysis. Amino acids in GRGDS (serine, glycine, arginine, and aspartic acid) were detected using o-phthalaldehyde (OPA) derivatization solution in borate buffer. The analysis was performed using an Agilent 1260 Infinity Quaternary LC System. Column conditions and elution gradients used were as previously described[6]. Samples were run on a reverse-phase Agilent C18-Extend column (3.5 μm, 4.6 x 75 mm) at 40 °C column temperature. Buffer A consisted of 10 mM sodium phosphate dibasic + 10 mM sodium tetraborate, pH 8.2, and buffer B consisted of 45% methanol, 45% acetonitrile, 10% water by volume. The flow rate of the elution gradient (0 min, 20% buffer B; 5.0 min, 60% buffer B; 9.5 min, 60% buffer B; 10.0 min, 20% buffer B) was 1 mL/min. Standard curves were generated for arginine over the concentration range of 0.01-1 mM.

TEM sample preparation and measurement was conducted as follows. 10 μL of nanoparticles at 1 mg/ mL in deionized water were added to a 200-mesh copper grid coated with a continuous carbon film. After 60 seconds, excess solution was wicked away, and 10 μL of negative staining solution, phosphotungstic acid, 1% aqueous solution was added to the TEM grid and immediately removed. Finally, 10 μL of the negative stain was then applied to the grid; excess stain was wicked away after 30 seconds. The grid was then dried at room temperature. Following that, the grid was mounted on a JEOL single tilt holder equipped in the TEM column. The specimens were cooled down by liquid-nitrogen and imaging on an JEOL 2100 FEG microscope was done using the minimum dose method that was essential to avoid sample damage under the electron beam. The microscope was operated at 200 kV and with a magnification in the ranges of 10,000~60,000 for assessing particle size and distribution. All images were recorded on a Gatan 2kx2k UltraScan CCD camera.

Dynamic light scattering measurements were conducted with a Malvern Zetasizer Nano ZS90 at 0.5 mg/ mL in various solvents (water, isotonic glucose, and cell culture media). The laser wavelength on the machine was 633 nm. The acquisition angle was 90°. Acquisition times were set to automatic on the machine and averaged 60-70 seconds per run. Three measurements were taken for each nanoparticle size (labeled and unlabeled), and the results were reported as an average and standard deviation.

Light transmission-based measurements were performed using a PowerWave HT, Bio-Tek microplate reader, while all other well-plate measurements were performed on a Tecan microplate reader. Specific wavelengths for each type of assay and well-plate types are detailed in the following sections.

Polymer and Nanoparticle Synthesis

Boc-protected-Poly(ethylene oxide) (NHBoc-PEG-OH): OH-PEG-NH$_2$ (400 mg, 8×10^{-5} mol, 5 kDa) was dissolved in 3.5 mL of dichloromethane (DCM). 78 μL of diisopropylethylamine (DIPEA , ~4×10^{-5} mol), and 62 μL of Boc anhydride (~2.7×10^{-4} mol) was added to the solution. The mixture was stirred for three hours at room temperature (RT). The polymer was precipitated in diethyl ether three times, resulting in a final yield of 91% (363 mg). Boc protection was confirmed *via* appearance of the tert-butyl protons at around 1.4-1.5 ppm *via* ^{1}H NMR spectroscopy.

Boc-Poly(ethylene oxide)-b-Poly(D,L-lactide-co-glycolide) (NHBoc-PEG-PLGA), Batch 1: The synthesis of NHBoc-PEG-PLGA was adapted from the literature[49], targeting a molecular weight of 25k-35k PLGA with a lactide: glycolide ratio between 55:45 and 60:40. This batch was scaled up to conduct a full animal study (Batch 2), which, like Batch 1, was characterized with ^{1}H NMR spectroscopy, gel permeation chromatography, amino acid analysis, dynamic light scattering and light transmission measurements in platelet-rich plasma to confirm functionality. The following procedure describes the synthesis of Batch 1, as well as all subsequent steps leading to the synthesis of GRGDS-PEG-PLGA. In a nitrogen glovebox, BocNH-PEG-OH (335 mg, 6.7×10^{-5} mol) was dissolved in 14 mL anhydrous DCM and left overnight on activated molecular sieves in an airtight container. Rac-lactide (1296 mg, 9×10^{-3} mol) was added to this solution, and the mixture was transferred to a round-bottomed flask with a magnetic stir bar and sealed with a rubber septum. Glycolide (878 mg, 7.6×10^{-3} mol) was dissolved in 4.5 ml DMF and taken up in a syringe. 22 μL of DBU was added to 2 mL of DCM and taken up in a second syringe. All materials were removed from the glovebox, and the DBU solution was added to the dissolved lactide and OH-PEG-NHBoc. This was immediately followed by infusion of the DMF-glycolide mixture *via* syringe pump at a rate of 45 μL/ min. The reaction was allowed to proceed at RT for 80 minutes before it was terminated with 16 mg of benzoic acid (2 equiv.). The polymer was precipitated in isopropanol twice and diethyl ether once, resulting in a final purified yield of 1.87 g (80.1%). The exact molecular weight (referenced to commercial 5 kDa PEG) as determined through NMR, was 33,072 Da of PLGA (LA: GA = 57.8: 42.2). The NMR spectrum for this batch (Batch 1) is shown in the Supporting Information.

Poly(D,L-lactide-co-glycolide)-b-Poly(ethylene oxide) (mPEG-PLGA): The synthesis of mPEG-PLGA was performed in a manner identical to that for BocNH-PEG-PLGA, with the only difference being that mPEG-OH was used instead of BocNH-PEG-OH. A final purified yield of 1.56 g was obtained (69.4%). The final molecular weight obtained was 28,833 Da of PLGA (LA: GA = 57.7: 42.3). The NMR spectrum is shown in the Supporting Information.

NH$_2$-Poly(ethylene oxide)-b-Poly(D,L-lactide-co-glycolide) (NH$_2$-PEG-b-PLGA): 1.85 g of BocNH-PEG-PLGA was dissolved in 20 mL of DCM and 20 mL of TFA. The solution was stirred overnight, with excess TFA and DCM removed using a vacuum oven. The resulting solid was redissolved in DCM and precipitated twice into diethyl ether, resulting in a final yield of 1.77 g (95.6%).

Carbonylimidazole-Poly(ethylene oxide)-b-Poly(D,L-lactide-co-glycolide) (carbonylimidazole-PEG-b-PLGA): The amine terminus of NH$_2$-PEG-PLGA was activated as described in literature[6]. In brief, 1.75 g of the polymer was dissolved in 14 mL of dioxane at 37 °C, along with 52.2 mg of CDI (6:1 molar excess). The solution was stirred for 3.5 hours before the polymer was precipitated in ether. A final purified yield of 1.5 g (85.7%) was obtained, and the activated polymer was used within 12 hours.

GRGDS-Poly(ethylene oxide)-b-Poly(D,L-lactide-co-glycolide) (GRGDS-PEG-b-PLGA): Carbonylimidazole-PEG-PLGA (1.5 g, ~36,000 g/ mol, 4.2×10^{-5} mol) was mixed with the GRGDS peptide (100 mg, 490 g/ mol, 5 equiv.) in 17 mL anhydrous DMSO and stirred for 48 hours. To remove excess peptide, the polymer solution was diluted with additional DMSO to a concentration of approximately 50 mg/ mL and dialyzed against deionized water for 72 hours (molecular weight cut-off (MWCO): 3,500 g/mol). The resultant slurry was lyophilized to yield 1.25 g of white solid (83.3% yield). This was stored at −20 °C until it was used in subsequent experiments.

Methoxy-Poly(ethylene oxide)-b-Poly(D,L-lactide-co-glycolide-Cy5 (mPEG-b-PLGA-Cy5): mPEG-b-PLGA-OH (400 mg, 1.14×10^{-5} mol, ~35,000 g/ mol), DMAP (0.56 mg, 4.56×10^{-6} mol, 0.4 equiv.), and Cy5 (5.9 mg, 1.14×10^{-5} mol, 1 equiv.) were dissolved in 7 mL DCM. DCC (18.8 mg, 9.12×10^{-5} mol, 8 equiv.) was dissolved in 1 mL of DCM and added dropwise to the mixture, which was stirred overnight at RT. The labeled polymer was precipitated twice in isopropanol and once in ether to remove excess dye. No further purification steps were made to isolate the conjugated polymer from unreacted mPEG-b-PLGA (a single batch of labeled polymer was used throughout the manuscript), and the crude yield was 360 mg (88.7%).

Methoxy-Poly(ethylene oxide)-b-Poly(D,L-lactide-co-glycolide-Cy7 (mPEG-b-PLGA-Cy7): The synthesis of mPEG-b-PLGA-Cy7 was performed in a manner identical to its Cy5 counterpart, with the only difference being the use of Cy7 instead of Cy5 (7.14 mg, 1.14×10^{-5} mol, 1 equiv.). A final purified yield of 352 mg was obtained (86.7%).

PLGA-b-PEG-GRGDS Nanoparticles: GRGDS-PEG-b-PLGA nanoparticles were synthesized through either nanoprecipitation or dialysis[6, 31]. In brief, the nanoparticles were

grouped into five size ranges as determined through dynamic light scattering (DLS): <100 nm, 110-130 nm, 140-220 nm, 250-400 nm, and 500-650 nm. These distinct size ranges were determined through multiple batches of nanoparticle synthesis, which was necessary in order to ensure consistent particle quality across *in vitro* and *in vivo* experiments spanning several months. With the exception of the 500-600 nm group, all other groups were synthesized through nanoprecipitation. Mixed nanoparticles were synthesized in a 20 mg/ ml stock solution by mixing equal volumes of small, intermediate, and large nanoparticles at their respective 20 mg/ ml stock concentrations. For these sizes, GRGDS-PEG-b-PLGA and pure PLGA (in a 5:1 mass ratio) were dissolved in a water-miscible solvent (DMF, THF, or acetonitrile) at predetermined concentrations, and the resulting solution was added dropwise to deionized water stirred at 700 rpm to form nanoparticles of varying sizes. Dialysis of GRGDS-PEG-b-PLGA at 8 mg/ mL in DMSO through a 3,500 g/ mol MWCO membrane resulted in nanoparticles measuring 500-600 nm. Table 1 summarizes the various solvents, polymer concentrations, and solvent: water ratios used to generate these different particle sizes.

Fluorescently-labeled (Cy7 or Cy5) GRGDS-PEG-b-PLGA Nanoparticles: Fluorescently-labeled nanoparticles were generated through the addition of a small amount of the crude labeled polymer, with the ratio of GRGDS-PEG-b-PLGA to mPEG-b-PLGA-Label to pure PLGA set at 4:1:1, ensuring that the ratio of PEG-PLGA to pure PLGA remained at 5:1 as noted in the previous section. The labeled nanoparticles were synthesized with the same procedure (nanoprecipitation or dialysis) as the unlabeled nanoparticles.

Blood Components Preparation

Citrated human whole blood was centrifuged at 200 x g for 20 min in a 15 mL conical tube. The supernatant, platelet rich plasma (PRP), was used in the aggregation, coagulation, flow cytometry, and surface binding tests described in the subsequent sections.

In vitro Particle Characterization and Evaluation of Hemostatic Efficacy

Platelet Aggregation Measurements—Platelet aggregation measurements were obtained as previously described in literature by incubating various nanoparticle sizes and concentrations with PRP and ADP in uncoated 96 well plates[6]. In brief, PLGA-b-PEG-GRGDS nanoparticles of various sizes were diluted to five concentrations from a stock solution of 20 mg/ mL in isotonic sucrose. This was accomplished by taking 3, 6, 15, 22.5, and 30 μL of the stock and adding isotonic sucrose to achieve final volumes of 45 μL. 270 μL of PRP was then added to each nanoparticle dilution before the mixture was combined with 30 μL of 0.1 mM ADP or saline (for negative controls). 100 μL of this final solution was added to each well. Sample absorbance was measured in a microplate reader set to 37 °C and read at 620 nm for 20 minutes, with agitation between measurements. Transmission measurements at 450 nm of Cy5-labeled nanoparticles were also collected to preclude the absorbance of Cy5 at 646 nm.

Coagulation Measurements—Coagulation measurements were obtained as previously described in the literature[6]. In brief, PLGA-b-PEG-GRGDS nanoparticles of various sizes

were diluted to the final concentration from a stock solution of 20 mg/mL in isotonic sucrose. This was accomplished by taking 3, 6, 15, 22.5, and 30 μL of the stock and adding isotonic sucrose to achieve final volumes of 45 μL. 15 μL of each dilution was added to a well in a 96 well plate, and all tests were performed in triplicate. 10 μL CaCl$_2$ was also added to each well, and 90 μL PRP was added to all wells using a multichannel pipette, where it was mixed by pipetting up and down. Transmission measurements at 650 nm were taken of the well plate in a microplate reader set to 37 °C over the span of 30 minutes. Coagulations measurements of Cy5-labeled nanoparticles were likewise conducted at 450 nm, as detailed in the previous section. All measurements were normalized to positive and negative controls at that specific wavelength.

Platelet Flow Cytometry—Sample Preparation—Flow cytometry was introduced as a quantitative method to evaluate the binding of hemostatic nanoparticles to activated platelets in PRP. Markers were selected from platelet flow cytometry studies conducted in the literature[50]. Prior to evaluating the complete size range, several concentrations and agonist combinations (ADP, thrombin, and/or collagen) were tested on a single particle size (<100 nm) in order to obtain a suitable range of concentrations and activation conditions. A suitable dilution of PRP (to prevent significant loss of aggregates compared to the quiescent platelets) was likewise determined using this particle size. In the optimized procedure, PRP was diluted by combining 150 μL of 15 mM GPRP-NH$_2$ anticoagulating peptide solution, 585 μL FACS buffer (0.9 wt% saline + 5% FBS), 15 μL 100 mM calcium chloride and 100 μL thrombin at 100 U/mL to 150 μL of PRP. A similar dilution of inactivated platelets for negative controls was made by replacing the addition of calcium chloride and thrombin with equivalent volumes of FACS buffer. 2 μL of nanoparticles at a specified concentration (either 20, 10, 5, or 1 mg/ mL in isotonic glucose) was then added to 20 μL of the diluted PRP mixtures (both activated and inactivated) to yield a final concentration of 2, 1, 5, or 1 mg/ mL NP per mL of diluted PRP. Nanoparticle-free activated (positive) controls and inactivated (negative) controls were also prepared at this stage by omitting the nanoparticle addition step. These solutions were incubated for 20 minutes under agitation at RT. All antibodies were diluted at a 1:5 ratio from the concentration at which they were provided before use (*e.g.* 20 μg / mL of anti-CD41-AF488, 20 μg/ mL of anti-CD2P-BV421, and 0.8 μg/mL of Annexin V-PE). Unstained and single-color controls were prepared by adding 15 μL of FACS buffer or 5 μL of diluted antibody solution and 10 μL FACS buffer to equalize volumes, whereas full-color samples were labeled by adding 5 μL of each diluted antibody. The samples were incubated at RT for 30 minutes in the dark, before the labeling was terminated by the addition of 500 μL 1% paraformaldehyde in 0.9 wt% saline.

Platelet Flow Cytometry—Data Acquisition and Analysis—Samples were analyzed using a FACS LSR II (BD Biosciences) equipped with FACSDIVA software and 4 lasers (405, 488, 561, and 640 nm). All samples were analyzed within an hour of preparation, and acquisition was performed until 10,000 events had been recorded using a temporary cell gate. The raw data (including events collected outside the size range of the cell gate) was then gated by selecting a population that excluded single-positive Cy5$^+$ events —which were indicative of free particle detection by the flow cytometer—followed by gating for CD41-positive cells to separate platelets form other cells or cell debris. From

this population the following metrics were evaluated: $CD62P^+$ / $CD41^+$, the percentage of activated platelets over all platelets; $Cy5^+$ / $CD41^+$, the percentage of particle-bound platelets; and finally, Annexin V / $CD62P^+$, the percentage of procoagulant platelets (which expose phosphatidylserine receptors that bind Annexin V) over all activated platelets. The experiment was repeated with three separate donors.

Particle-Platelet Surface Binding Assay—Nanoparticle binding to platelets adherent to a surface was evaluated by adapting a generic nanoparticle uptake assay. Two concentrations of Cy5-labeled hemostatic nanoparticles to PRP + agonist were selected: 2 mg/mL and 1 mg/mL. Mixed nanoparticles were tested at a concentration of 1 mg/ mL in platelet-rich-plasma with a freshly synthesized batch of small, intermediate, and large nanoparticle sizes. 180 μL of PRP was mixed with 20 μL of ADP or saline (negative/inactive platelet controls). 54 μL of this mixture was added to each well in a black 384-well cell-treated plate. Following a 10-min incubation step, 6 μL of concentrated nanoparticle solution (at either 20 mg/ mL or 10 mg/mL) was also added to each well. The well plate was incubated at 37 °C under agitation (~200 rpm) for 20 min, identical to the conditions under which platelet aggregation was evaluated. Subsequently, the solution was carefully aspirated from the wells and washed twice with PBS to remove weakly adherent or nonadherent platelets and nanoparticles. 15 μL of cold RIPA lysis and extraction buffer was added to each well and left for 5 minutes, before the plate was read on a Tecan microplate reader at 630 nm excitation and 670 nm emission. Nine replicates were collected for this measurement. A variation of this assay was performed with wells coated with collagen gels. In brief, rat tail collagen was dissolved in 0.1M acetic acid at a concentration of 0.1 mg/ mL. 2 μL of 1 M NaOH was added to each well in a 384-well plate with a multichannel pipette, after which 18 μL of the collagen solution was also added to the wells and mixed vigorously. The plate was first agitated overnight on a shaker at 200 rpm and allowed to fully dry over the next 36 hours. As collagen was a potent platelet agonist, nanoparticles in isotonic sucrose were substituted as negative controls (in place of inactive platelets on cell-treated surfaces) to evaluate the degree of nonspecific particle binding to collagen. Six replicates were collected for this measurement.

Platelet Binding/ Aggregate Quantification Assay—The effect of nanoparticle size on the total amount of platelet aggregation/ binding to a surface was evaluated by a lactate dehydrogenase (LDH) assay as modified from literature[51]. In brief, unlabeled nanoparticles were mixed with PRP and agonist/saline and incubated under agitation in the same manner described in the particle-platelet binding assay. After two washing steps to remove weakly adherent or nonadherent platelets and particles, the platelets were lysed with cold RIPA lysis buffer (50 μL per well). Dilutions of this lysate were analyzed *via* manufacturer's instructions for the Pierce LDH cytotoxicity assay; in brief, a calibration curve was constructed by incubating 12.5 μL aliquots of dilutions from the positive control with 12.5 μL of LDH reaction mixture for 30 minutes at room temperature. Following this step, 12.5 μL of stop solution was added to terminate the colormetric reaction. The plate's absorbance was then measured at 490 nm and 680 nm, with the final results calculated by subtracting the readings at 680 nm for those at 490 nm. 12 replicates were collected for this measurement, after a pilot study on six replicates was found to show a trend but lower

significance. This assay was not repeated on collagen gel due to its role as a potent platelet agonist, which would cause inactive platelets to aggregate even without the presence of ADP.

Particle Stability Measurements—The stability of particle sizes over time was evaluated by incubating aliquots of particles at 1 mg/ml in 37 °C α–MEM cell culture media. The concentration corresponded to a peptide content at which all nanoparticle sizes showed an increase in platelet aggregation. The samples were removed at 1hr, 3hr, 5 hr, 36 hr, and 72 hr time points and measured with DLS to detect any changes in size over the incubation period. A truncated version of this test was repeated with dye-labeled nanoparticles (measured at 1.5 hr and 3 hrs). As Cy7 and Cy5 were both chemically conjugated to PEG-PLGA, minimal release of dye was expected. A dye release test was nevertheless conducted by incubating 20 μL aliquots of labeled nanoparticles in isotonic glucose to 180 μL α–MEM cell culture media at 37 °C and agitated at 200 rpm on a shaker. The samples were likewise removed at 1.5 hrs and 3 hrs, after which the particles were diluted with water and separated from free dye using an ultrafiltration membrane. The flow through and concentrate were measured on a plate reader against nanoparticle standards in media. To evaluate the stability of the bound peptide, nanoparticles were suspended in PRP at a stock concentration of 6.67 mg/ ml by combining 20 μl of 20 mg/ mL stock solution with 40 μl of PRP. This solution was incubated overnight at 37 °C (~12 hours) under agitation. 9 μL of this solution was added to 45 μL PRP from the same person and 6 μL of ADP, while control wells received 3μL of fresh nanoparticle solution, 48 μL PRP, and 6μL of ADP or 3 μL of saline, 48 μL PRP, and 6μL of ADP. Six replicates were performed for each measurement, and final transmission values were normalized to that of the particle-free control.

Coagulation activity assays: The effect of hemostatic nanoparticles on coagulation factors was evaluated through enzyme concentration assays for FIXa (contact/ intrinsic activation pathway), Tissue Factor (Tissue Factor/ extrinsic activation pathway), and thrombin (common pathway). In brief, small, intermediate, large, and mixed nanoparticles were incubated in platelet-rich-plasma at a concentration of 1 mg/ mL for 30 minutes. Platelet-free-plasma was then obtained by centrifuging the solution at 3,000 rcf and diluted according to manufacturer's instructions (between 1:2 and 1:10). All assays were conducted and analyzed according to manufacturer's instructions using a Tecan microplate reader (absorbance at 405 nm for Tissue Factor and Ex/Em at 350/450 for FIXa and thrombin).

In vivo Particle Characterization and Evaluations of Hemostatic Efficacy

In Vivo *Imaging of Hemostatic Nanoparticles in Uninjured Mice—*Female BALB/c mice (10-12 weeks old, 20-22g) were used in accordance with procedures approved by the MIT Division of Comparative Medicine and the Institutional Animal Care and Use Committee (IACUC) of MIT. Animals had *ad-libitum* access to both food and water until the time of the procedure. The animals were randomized into groups of six, for a total of six groups (five sizes and a free dye control). Each group was then split into two subgroups, one for blood collection (BC) and the other for *in vivo* imaging (IVIS, Caliper Instruments). The animals each received one 100-μL injection of Cy7-hemostatic nanoparticles at a

concentration of 20 mg/ mL in isotonic glucose through the tail vein or one 100-μL injection of free dye in isotonic glucose at a concentration that matched the nanoparticle fluorescence when read on a Tecan microplate reader. Immediately following the injection, 30 μL of blood was collected *via* cheek bleed with a 26-gauge needle from each of the three animals. All six animals were then anesthetized *via* isoflurane before being imaged *via* IVIS (Ex. 745/ Em. 800 nm). Blood collection was repeated on the BC group at t = 30, 75, 120, and 180 min. The IVIS group was likewise anesthetized and imaged at the same time points and euthanized at the end of the 3h experiment by carbon dioxide inhalation. Subsequently, the liver, lungs, spleen, kidneys, and heart were harvested from these mice, weighed, and imaged with IVIS to quantify fluorescent nanoparticle content. The BC group was observed for two weeks following the experiment and monitored for any deleterious side effects. Blood samples (anticoagulated with EDTA) were diluted to half their starting concentration in PBS and imaged on IVIS alongside a free dye standard curve; they were also read on a Tecan microplate reader (Ex. 745/ Em. 780 nm) to quantify remaining fluorescence.

In Vivo *Rat Model of Surgically Induced Inferior Vena Cava Injury*—Male Sprague-Dawley rats (450-600g) were used in accordance with procedures approved by the Animal Care and Use Committee (IACUC) of Massachusetts General Hospital. Five rats were used to test the reproducibility of the inferior vena cava (IVC) injury model, targeting a >50% mortality rate within two hours of the injury upon administration of the isotonic saline control. These were included in the final number of rats in the control group (n = 15). Ten animals were included in each trial group of unlabeled nanoparticle (<100 nm, ~180 nm, ~500 nm, and an unfunctionalized 180 nm control), with three additional animals used to perform biodistribution studies *via* Cy7-labeled nanoparticles per trial group (total of n = 13). Both saline, various-sized PLGA-*b*-PEG-GRGDS nanoparticles at 20 mg/mL (2 ml), and unfunctionalized nanoparticles were delivered in a single isotonic dose immediately following the injury, and the survival time, mortality rate, and total fluid loss by weight were recorded. No additional fluid resuscitation was administered throughout the course of the two-hour observation period.

Animal preparation and surgery were performed according to the following procedure. An inguinal incision was performed following anesthesia with inhaled isoflurane (2.5%), and the left femoral vein was cannulated with a 24G catheter, which was flushed with 0.2 ml of isotonic saline. A midline laparotomy was performed, and the IVC was exposed. A double-puncture (perforating) IVC injury was created using an 18-gauge catheter and carefully withdrawn, resulting in rapid exsanguination. Immediately following the removal of the catheter, normal saline, various-sized GRGDS nanoparticles, or unfunctionalized nanoparticles the same size as the best-performing GRGDS nanoparticle group were administered intravenously through the femoral catheter (time 0). The animal was observed for an additional two hours, or until mortality (as determined by cessation of breathing for at least 15 minutes.) Pre-weighed gauzes were placed next to the injury site to collect blood. Animals that remained alive at the endpoint of the experiment were euthanized *via* exsanguination, after the gauzes were collected to calculate blood loss. The kidneys, spleen, heart, lungs, clots, liver, uninjured [right] femoral vein (FV) and IVC (1 cm segment proximal to the injury, and another 1 cm segment at the injury site) were harvested from all

animals with labeled nanoparticles and fixed in neutral buffered formalin for biodistribution studies. As done with the uninjured murine study, biodistribution was quantified *via* imaging these organs on the IVIS.

Supplementary Material

Refer to Web version on PubMed Central for supplementary material.

ACKNOWLEDGMENTS

REFERENCES

1. Donley ER; Loyd JW, Hemorrhage Control. StatPearls Publishing Copyright © 2021, StatPearls Publishing LLC.: Treasure Island (FL), 2022.

2. Chiara O; Cimbanassi S; Pitidis A; Vesconi S, Preventable Trauma Deaths: From Panel Review to Population Based-Studies. World J Emerg Surg 2006, 1, 12–12. [PubMed: 16759417]

3. Beck B; Smith K; Mercier E; Bernard S; Jones C; Meadley B; Clair TS; Jennings PA; Nehme Z; Burke M; Bassed R; Fitzgerald M; Judson R; Teague W; Mitra B; Mathew J; Buck A; Varma D; Gabbe B; Bray J; McLellan S; Ford J; Siedenburg J; Cameron P, Potentially Preventable Trauma Deaths: A Retrospective Review. Injury 2019, 50 (5), 1009–1016. [PubMed: 30898389]

4. Gholipour C; Rad BS; Vahdati SS; Ghaffarzad A; Masoud A, Evaluation of Preventable Trauma Death in Emergency Department of Imam Reza Hospital. World J Emerg Med 2016, 7 (2), 135–137. [PubMed: 27313809]

5. Kisat M; Morrison JJ; Hashmi ZG; Efron DT; Rasmussen TE; Haider AH, Epidemiology and Outcomes of Non-Compressible Torso Hemorrhage. J. Surg. Res 2013, 184 (1), 414–421. [PubMed: 23831230]

6. Gkikas M; Peponis T; Mesar T; Hong C; Avery RK; Roussakis E; Yoo H-J; Parakh A; Patino M; Sahani DV; Watkins MT; Oklu R; Evans CL; Albadawi H; Velmahos G; Olsen BD, Systemically Administered Hemostatic Nanoparticles for Identification and Treatment of Internal Bleeding. ACS Biomaterials Science & Engineering 2019, 5 (5), 2563–2576. [PubMed: 33405762]

7. Tasu JP; Vesselle G; Herpe G; Ferrie JC; Chan P; Boucebci S; Velasco S, Postoperative Abdominal Bleeding. Diagnostic and interventional imaging 2015, 96 (7), 823–831. [PubMed: 26078019]

8. Tchaou BA; Savi de Tové K-M; Sissinto-Savi de Tové Y; Djomga ATC; Aguemon A-R; Massougbodji A; Chippaux J-P, Contribution of Ultrasonography to the Diagnosis of Internal Bleeding in Snakebite Envenomation. J Venom Anim Toxins Incl Trop Dis 2016, 22, 13–13. [PubMed: 26989403]

9. Carr ME Jr., Monitoring of Hemostasis in Combat Trauma Patients. Mil. Med 2004, 169 (12 Suppl), 11–5, 4.

10. Chan LW; Wang X; Wei H; Pozzo LD; White NJ; Pun SH, A Synthetic Fibrin Cross-Linking Polymer for Modulating Clot Properties and Inducing Hemostasis. Science Translational Medicine 2015, 7 (277), 277ra29.

11. Shukla M; Sekhon UDS; Betapudi V; Li W; Hickman DA; Pawlowski CL; Dyer MR; Neal MD; McCrae KR; Gupta AS, In Vitro Characterization of Synthoplate(Tm) (Synthetic Platelet) Technology and Its in Vivo Evaluation in Severely Thrombocytopenic Mice. Journal of thrombosis and haemostasis : JTH 2017, 15 (2), 375–387. [PubMed: 27925685]

12. Okamura Y; Takeoka S; Teramura Y; Maruyama H; Tsuchida E; Handa M; Ikeda Y, Hemostatic Effects of Fibrinogen Γ-Chain Dodecapeptide-Conjugated Polymerized Albumin Particles in Vitro and in Vivo. Transfusion 2005, 45 (7), 1221–1228. [PubMed: 15987370]

13. Lashof-Sullivan MM; Shoffstall E; Atkins KT; Keane N; Bir C; VandeVord P; Lavik EB, Intravenously Administered Nanoparticles Increase Survival Following Blast Trauma. Proc Natl Acad Sci U S A 2014, 111 (28), 10293–8. [PubMed: 24982180]

14. Bertram JP; Williams CA; Robinson R; Segal SS; Flynn NT; Lavik EB, Intravenous Hemostat: Nanotechnology to Halt Bleeding. Science Translational Medicine 2009, 1 (11), 11ra22.

15. Shoffstall AJ; Atkins KT; Groynom RE; Varley ME; Everhart LM; Lashof-Sullivan MM; Martyn-Dow B; Butler RS; Ustin JS; Lavik EB, Intravenous Hemostatic Nanoparticles Increase Survival Following Blunt Trauma Injury. Biomacromolecules 2012, 13 (11), 3850–3857. [PubMed: 22998772]

16. Lashof-Sullivan M; Holland M; Groynom R; Campbell D; Shoffstall A; Lavik E, Hemostatic Nanoparticles Improve Survival Following Blunt Trauma Even after 1 Week Incubation at 50 (°)C. ACS biomaterials science & engineering 2016, 2 (3), 385–392. [PubMed: 27672679]

17. Onwukwe C; Maisha N; Holland M; Varley M; Groynom R; Hickman D; Uppal N; Shoffstall A; Ustin J; Lavik E, Engineering Intravenously Administered Nanoparticles to Reduce Infusion Reaction and Stop Bleeding in a Large Animal Model of Trauma. Bioconjugate Chem. 2018, 29 (7), 2436–2447.

18. Chan LW; White NJ; Pun SH, Synthetic Strategies for Engineering Intravenous Hemostats. Bioconjugate Chem. 2015, 26 (7), 1224–1236.

19. Anselmo AC; Modery-Pawlowski CL; Menegatti S; Kumar S; Vogus DR; Tian LL; Chen M; Squires TM; Sen Gupta A; Mitragotri S, Platelet-Like Nanoparticles: Mimicking Shape, Flexibility, and Surface Biology of Platelets to Target Vascular Injuries. ACS Nano 2014, 8 (11), 11243–11253. [PubMed: 25318048]

20. Singh R; Lillard JW Jr., Nanoparticle-Based Targeted Drug Delivery. Exp Mol Pathol 2009, 86 (3), 215–223. [PubMed: 19186176]

21. Blanco E; Shen H; Ferrari M, Principles of Nanoparticle Design for Overcoming Biological Barriers to Drug Delivery. Nat Biotech 2015, 33 (9), 941–951.

22. Perry JL; Reuter KG; Luft JC; Pecot CV; Zamboni W; DeSimone JM, Mediating Passive Tumor Accumulation through Particle Size, Tumor Type, and Location. Nano Lett. 2017, 17 (5), 2879–2886. [PubMed: 28287740]

23. Sykes EA; Chen J; Zheng G; Chan WCW, Investigating the Impact of Nanoparticle Size on Active and Passive Tumor Targeting Efficiency. ACS Nano 2014, 8 (6), 5696–5706. [PubMed: 24821383]

24. Alexis F; Pridgen E; Molnar LK; Farokhzad OC, Factors Affecting the Clearance and Biodistribution of Polymeric Nanoparticles. Mol Pharm 2008, 5 (4), 505–515. [PubMed: 18672949]

25. Shilo M; Sharon A; Baranes K; Motiei M; Lellouche J-PM; Popovtzer R, The Effect of Nanoparticle Size on the Probability to Cross the Blood-Brain Barrier: An in-Vitro Endothelial Cell Model. Journal of Nanobiotechnology 2015, 13 (1), 19. [PubMed: 25880565]

26. Rogers NJ; Jeffery HC; Claire S; Lewis DJ; Zikeli G; Hodges NJ; Egginton S; Nash GB; Pikramenou Z, Tailoring Iridium Luminescence and Gold Nanoparticle Size for Imaging of Microvascular Blood Flow. Nanomedicine 2017, 12 (22), 2725–2740. [PubMed: 28960141]

27. Shoffstall AJ; Everhart LM; Varley ME; Soehnlen ES; Shick AM; Ustin JS; Lavik EB, Tuning Ligand Density on Intravenous Hemostatic Nanoparticles Dramatically Increases Survival Following Blunt Trauma. Biomacromolecules 2013, 14 (8), 2790–2797. [PubMed: 23841817]

28. Looney M, Platelet Biogenesis in the Lung Circulation. Blood 2018, 132 (Suppl 1), SCI–22.

29. Eisinger F; Patzelt J; Langer HF, The Platelet Response to Tissue Injury. Frontiers in Medicine 2018, 5 (317).

30. Modery-Pawlowski CL; Tian LL; Ravikumar M; Wong TL; Gupta AS, In vitro and In vivo Hemostatic Capabilities of a Functionally Integrated Platelet-Mimetic Liposomal Nanoconstruct. Biomaterials 2013, 34 (12), 3031–3041. [PubMed: 23357371]

31. Cheng J; Teply BA; Sherifi I; Sung J; Luther G; Gu FX; Levy-Nissenbaum E; Radovic-Moreno AF; Langer R; Farokhzad OC, Formulation of Functionalized Plga-Peg Nanoparticles for in Vivo Targeted Drug Delivery. Biomaterials 2007, 28 (5), 869–876. [PubMed: 17055572]

32. Ferenz KB; Waack IN; Laudien J; Mayer C; Broecker-Preuss M; Groot H. d.; Kirsch M, Safety of Poly (Ethylene Glycol)-Coated Perfluorodecalin-Filled Poly (Lactide-Co-Glycolide) Microcapsules Following Intravenous Administration of High Amounts in Rats. Results in Pharma Sciences 2014, 4, 8–18. [PubMed: 25756002]

33. Battaglia L; Ugazio E, Lipid Nano- and Microparticles: An Overview of Patent-Related Research. Journal of Nanomaterials 2019, 2019, 2834941.

34. Martin FJ; Melnik K; West T; Shapiro J; Cohen M; Boiarski AA; Ferrari M, Acute Toxicity of Intravenously Administered Microfabricated Silicon Dioxide Drug Delivery Particles in Mice: Preliminary Findings. Drugs in R&D 2005, 6 (2), 71–81. [PubMed: 15818779]

35. Chisholm CF; Behnke W; Pokhilchuk Y; Frazer-Abel AA; Randolph TW, Subvisible Particles in Ivig Formulations Activate Complement in Human Serum. J. Pharm. Sci 2020, 109 (1), 558–565. [PubMed: 31672401]

36. He Z; Huang J; Xu Y; Zhang X; Teng Y; Huang C; Wu Y; Zhang X; Zhang H; Sun W, Co-Delivery of Cisplatin and Paclitaxel by Folic Acid Conjugated Amphiphilic Peg-Plga Copolymer Nanoparticles for the Treatment of Non-Small Lung Cancer. Oncotarget 2015, 6 (39).

37. Mares AG; Pacassoni G; Marti JS; Pujals S; Albertazzi L, Formulation of Tunable Size Plga-Peg Nanoparticles for Drug Delivery Using Microfluidic Technology. PLOS ONE 2021, 16 (6), e0251821. [PubMed: 34143792]

38. Biorender Adapted from "Zetasizer Nano Zs", "Incubated Stackable Shaker", and "Centrifugal Filter", by Biorender.Com (2021). Retrieved from Https://App.Biorender.Com/Biorender-Templates.

39. Biorender Adapted from "Platelet (Active)", by Biorender.Com (2021). Retrieved from Https://App.Biorender.Com/Biorender-Templates.

40. Decuzzi P; Gentile F; Granaldi A; Curcio A; Causa F; Indolfi C; Netti P; Ferrari M, Flow Chamber Analysis of Size Effects in the Adhesion of Spherical Particles. Int J Nanomedicine 2007, 2 (4), 689–696. [PubMed: 18203435]

41. Patil VRS; Campbell CJ; Yun YH; Slack SM; Goetz DJ, Particle Diameter Influences Adhesion under Flow. Biophys. J 2001, 80 (4), 1733–1743. [PubMed: 11259287]

42. Biorender Adapted from "Mouse (Supine)", by Biorender.Com (2021). Retrieved from Https://App.Biorender.Com/Biorender-Templates.

43. Lundy DJ; Chen K-H; Toh EKW; Hsieh PCH, Distribution of Systemically Administered Nanoparticles Reveals a Size-Dependent Effect Immediately Following Cardiac Ischaemia-Reperfusion Injury. Scientific Reports 2016, 6, 25613. [PubMed: 27161857]

44. Prokop A; Davidson JM, Nanovehicular Intracellular Delivery Systems. J. Pharm. Sci 2008, 97 (9), 3518–3590. [PubMed: 18200527]

45. Lawrensia S; Khan YS, Inferior Vena Cava Syndrome. StatPearls Publishing Copyright © 2021, StatPearls Publishing LLC.: Treasure Island (FL), 2021.

46. Kassassir H; Siewiera K; Przygodzki T; Labieniec-Watala M; Watala C, Flow Cytometry. IntechOpen Limited: London (UK), 2016.

47. Thon JN; Italiano JE, Platelet Formation. Semin Hematol 2010, 47 (3), 220–226. [PubMed: 20620432]

48. Gao Y; Sarode A; Kokoroskos N; Ukidve A; Zhao Z; Guo S; Flaumenhaft R; Gupta AS; Saillant N; Mitragotri S, A Polymer-Based Systemic Hemostatic Agent. Science Advances 2020, 6 (31), eaba0588. [PubMed: 32775633]

49. Qian H; Wohl AR; Crow JT; Macosko CW; Hoye TR, A Strategy for Control of "Random" Copolymerization of Lactide and Glycolide: Application to Synthesis of Peg-B-Plga Block Polymers Having Narrow Dispersity. Macromolecules 2011, 44 (18), 7132–7140. [PubMed: 22287809]

50. Södergren AL; Ramström S, Platelet Subpopulations Remain Despite Strong Dual Agonist Stimulation and Can Be Characterised Using a Novel Six-Colour Flow Cytometry Protocol. Scientific reports 2018, 8 (1), 1441–1441. [PubMed: 29362366]

51. Park JY; Gemmell CH; Davies JE, Platelet Interactions with Titanium: Modulation of Platelet Activity by Surface Topography. Biomaterials 2001, 22 (19), 2671–82. [PubMed: 11519787]
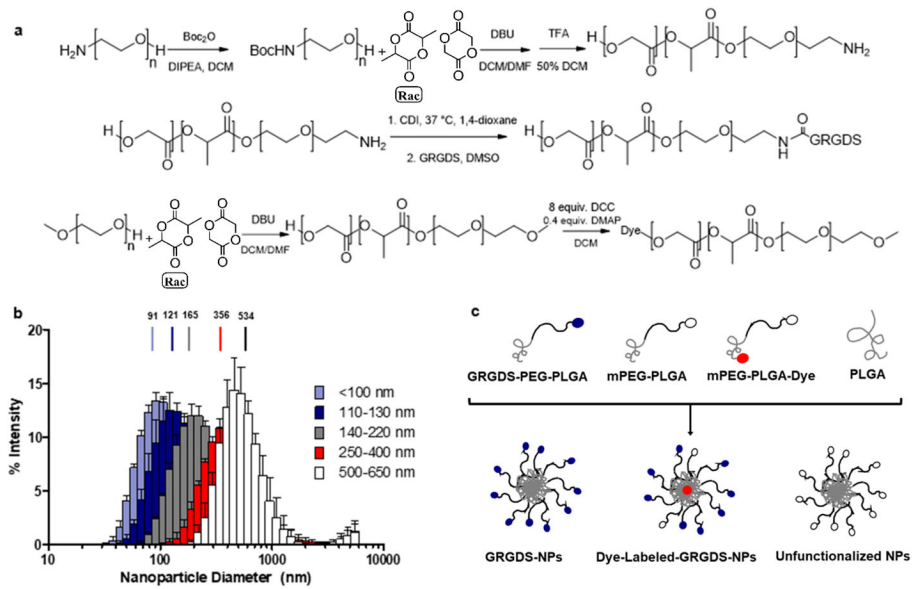
Figure 1. Polymer synthesis and nanoparticle formulation and characterization.
(a) Synthesis scheme of GRGDS-functionalized PEG-b-PLGA. (b) Particle size distributions of unlabeled particles, with z-averages of each size range noted. (c) Formulations of unlabeled, dye-labeled, and unfunctionalized NPs from starting materials (commercial PLGA, synthesized mPEG-PLGA, synthesized Cy5/Cy7 conjugated mPEG-PLGA, and GRGDS-PEG-PLGA).
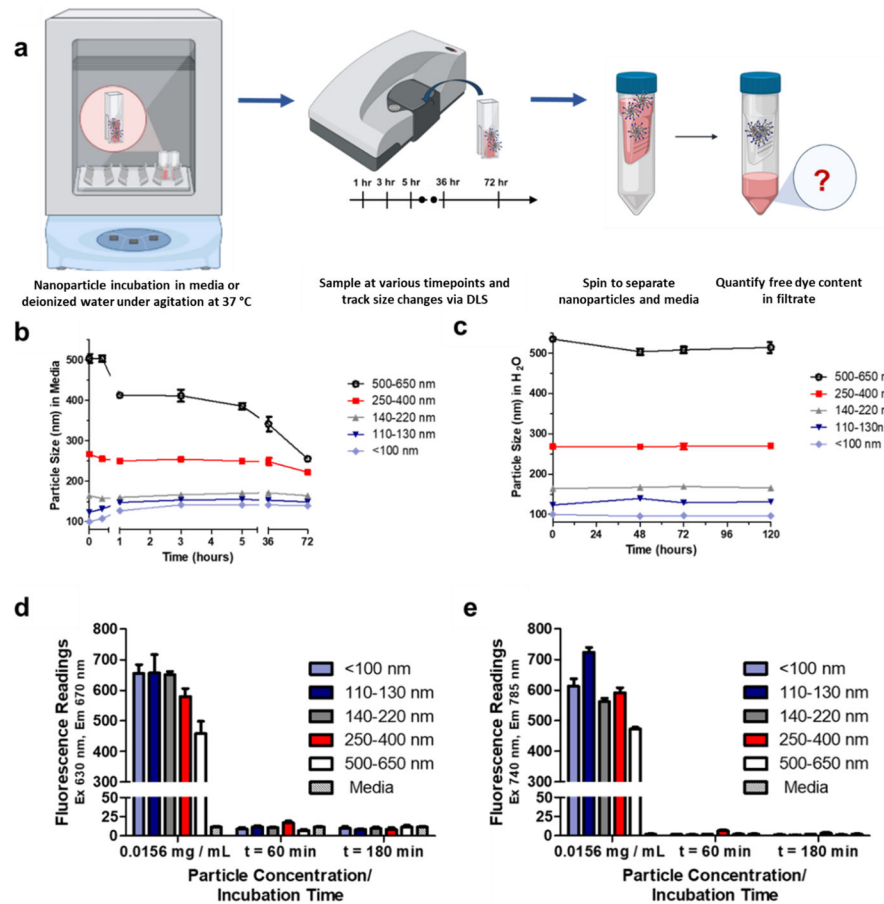
Figure 2. Stability of nanoparticle size and dye retention over time.
(a)Particle size changes over time in cell culture media at 37 °C (b) Particle size changes over time in water at 37 °C (c) Retention of Cy5 dye in Cy5-labeled nanoparticles (d) Retention of Cy7 dye in Cy7-labeled nanoparticles. The concentration represents approximately 1% of the initial nanoparticle concentration incubated (1.5 mg/ mL media). Adapted from Biorender[38].
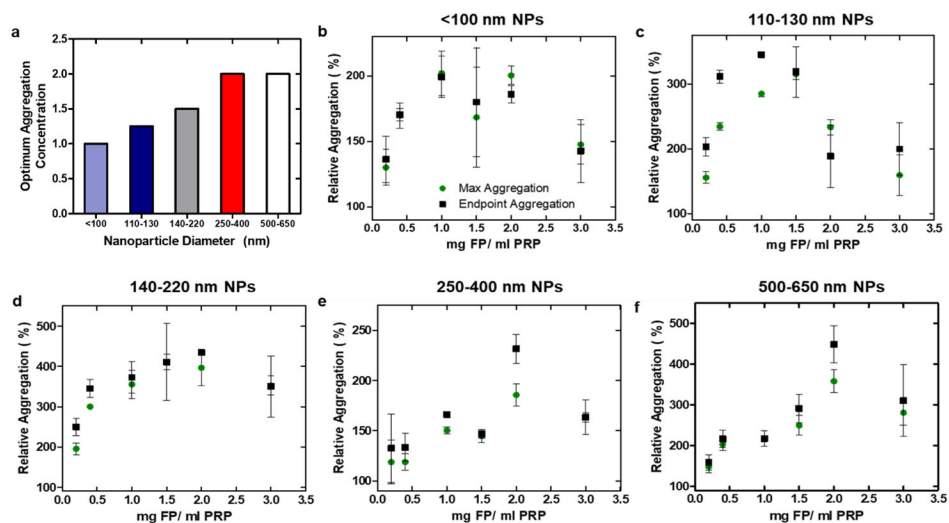
Figure 3. Particle size and concentration modulate platelet aggregation.
Absorbance measurements of PRP and particle combinations were taken on a microplate reader and converted to transmission, where the increase in transmission reflects the generation of platelet aggregation. (a) Concentrations at which optimum aggregation was observed. If maximum and endpoint averages reached their respective maxima at two consecutive concentrations, an average between the two concentration was reported. (b) – (f) Maximum and endpoint aggregation of the five nanoparticle size groups, normalized to the positive control (PRP + ADP). This experiment was conducted on a single batch of plasma.
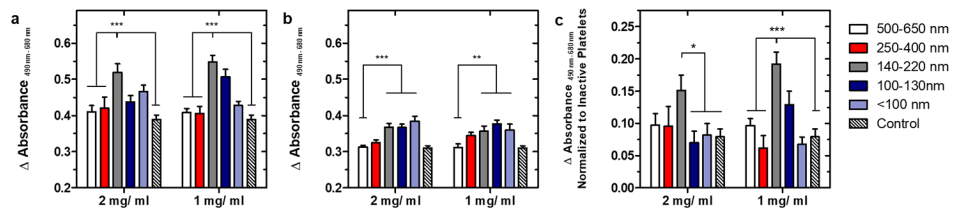
Figure 4. Quantifying total number of platelets bound when aggregated *via* the lactate dehydrogenase assay.

4a. Absorbance readings when incubated with activated platelets. Percentage increase relative to ADP-only positive control (ranked from largest to smallest size group) as calculated from calibration curve are 17%, 26%, 131%, 40% and 64% at 2mg FP/ mL PRP, and 16%, 14%, 133%, 98%, and 32% at 1 mg FP/ mL PRP. 4b. Absorbance readings when incubated with quiescent platelets. Percentage increase relative to negative control (ranked from largest to smallest size group) are 5%, 36%, 141%, 139%, and 181% at 2 mg FP/mL PRP and 4%, 83%, 113%, 164%, and 122% at 1 mg FP/ mL PRP. 4c. Absorbance readings of activated platelets normalized to nonspecific binding to quiescent platelets. For all tests, n = 12, ns: p > 0.05; *: p $\leq$ 0.05; **: p $\leq$ 0.01; ***: p $\leq$ 0.001 as determined through 2-way ANOVA with Bonferroni post-tests.
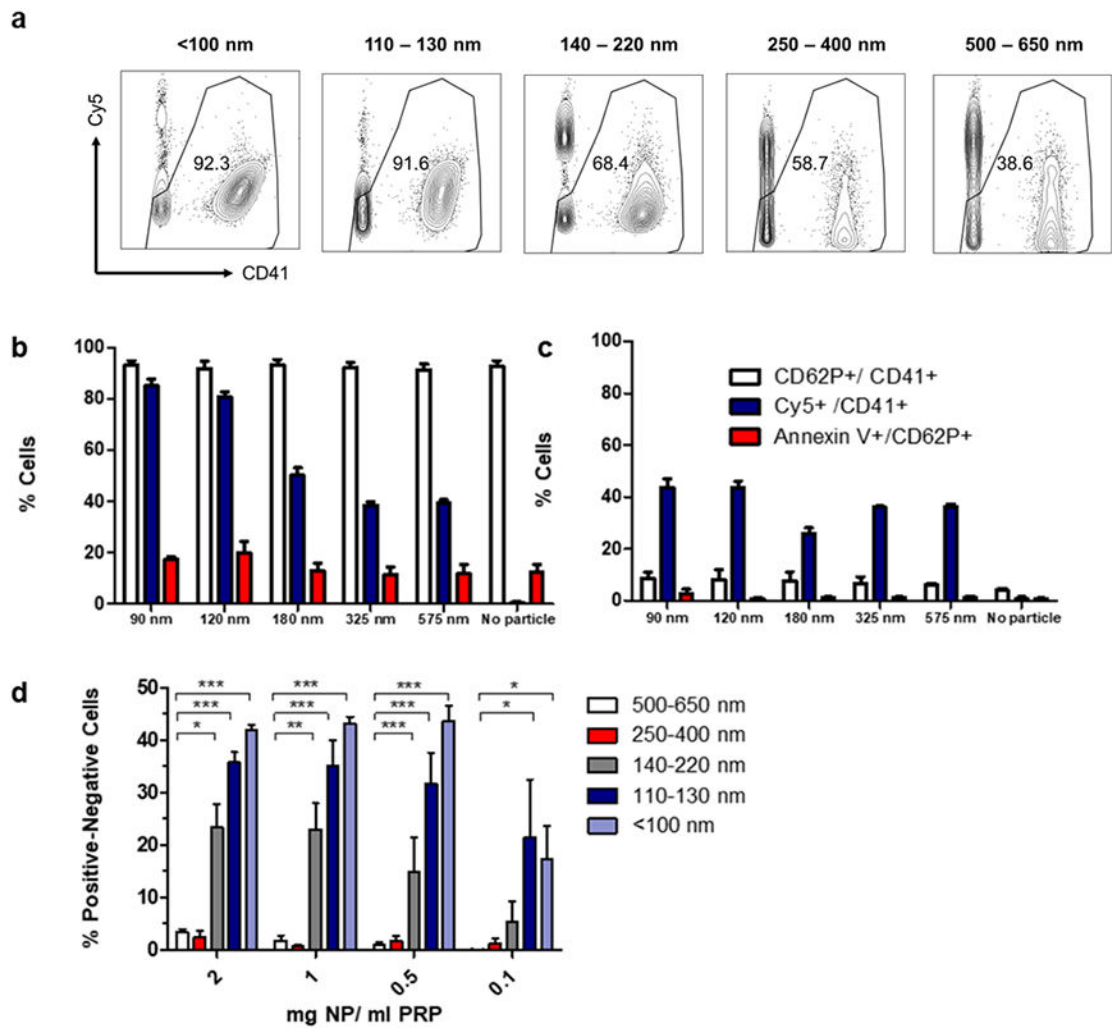
Figure 5. Effect of particle size on platelet binding under flow.
(a) Representative dot plots of gating strategy to isolate platelets (removal of Cy5+ only events and gating by CD41+). (b) Expression of various markers (CD41, CD62P, Annexin V) and binding of nanoparticles to active platelets (Cy5+/CD41+) at 1 mg NP/ ml PRP. (c) Expression of various markers (CD41, CD62P, Annexin V) and binding of nanoparticles to inactive platelets (Cy5+/CD41+). (d) Binding of different-sized nanoparticles to platelets at various concentrations (n = 3, ns: $p > 0.05$; *: $p \le 0.05$; **: $p \le 0.01$; ***: $p \le 0.001$) as determined through 2-way ANOVA with Bonferroni post-tests.
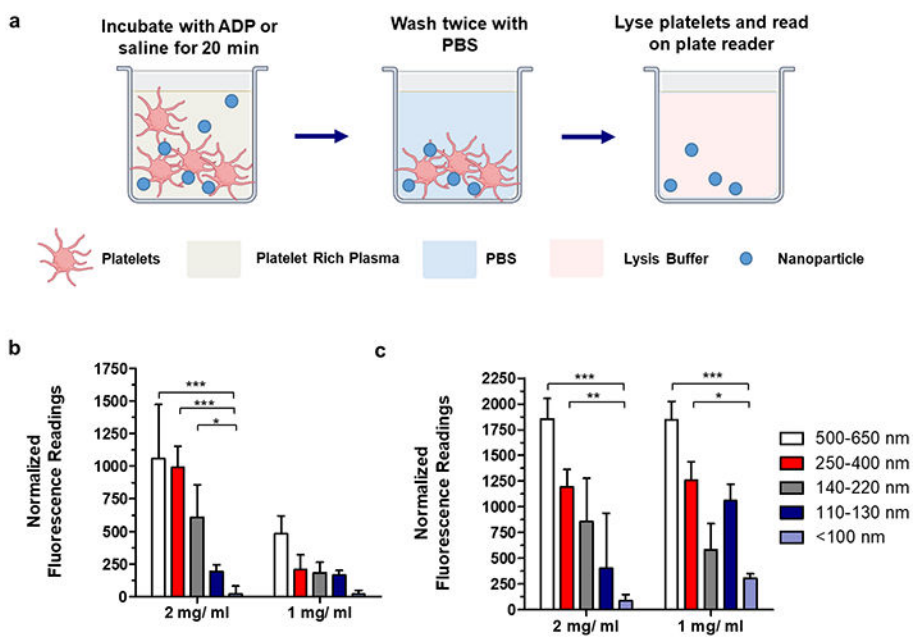
**Figure 6. Evaluating surface binding of nanoparticles.**
(a): Procedure for particle incubation with PRP; (b) Binding of nanoparticles to active platelets on cell-treated surface (normalized to particles on inactive platelets on cell-treated surfaces, 9 replicates). (c) Binding of nanoparticles to active platelets on collagen (normalized to particle binding on collagen surface without PRP, 6 replicates. For all tests, ns: $p > 0.05$; *: $p < 0.05$; **: $p < 0.01$; ***: $p < 0.001$ as determined through 2-way ANOVA with Bonferroni post-tests. Adapted from Biorender [39]
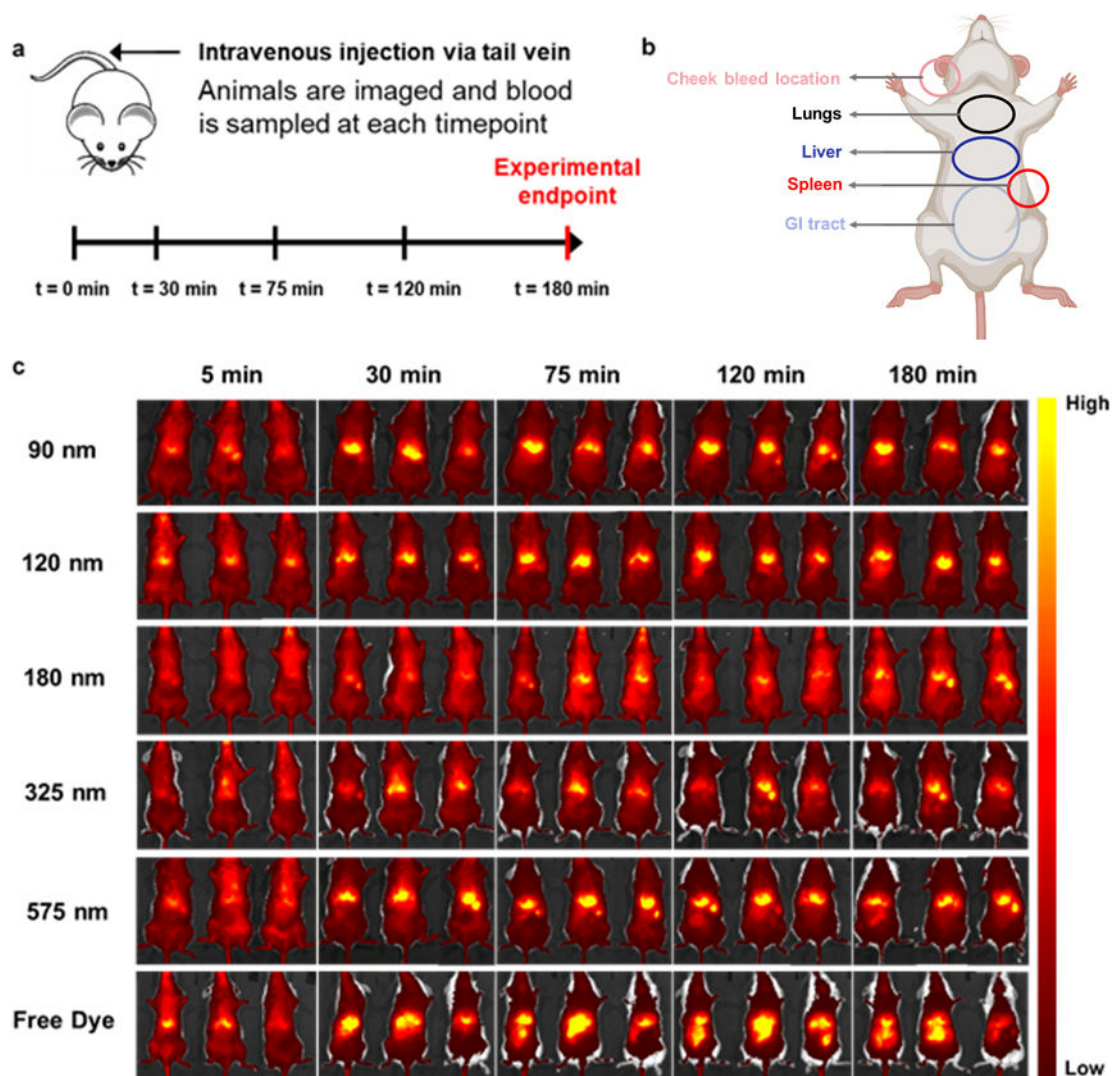
Figure 7. *In vivo* biodistribution of Cy7-labeled nanoparticles and a free dye control in BALB/c mice.

(a). Dosing, blood sampling, and imaging schedule. (b) Overview of organ locations in mouse. Adapted from Biorender[42] (c). Live imaging of Cy7-labeled hemostatic nanoparticles and free dye control over three hours. Sizes are expressed as the average of each size range for space considerations. Dark red/black denote lower levels of fluorescence, while yellow indicates accumulation in a particular area.
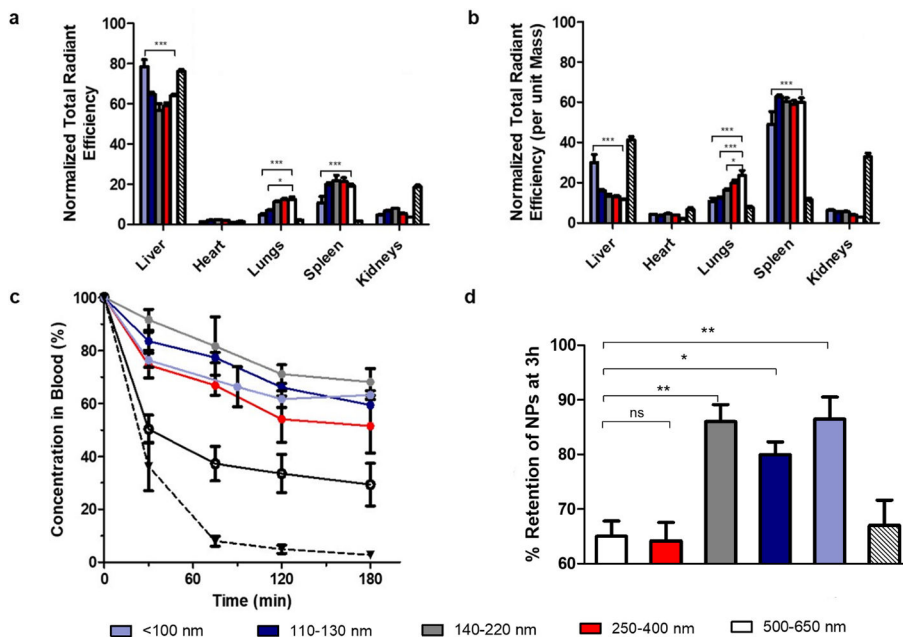
Figure 8. Organ biodistribution of Cy7-labeled nanoparticles and a free dye control in BALB/c mice.

(a) Organ biodistribution data *not* normalized to organ mass, normalized to total radiant efficiency over all organs measured (b). Organ biodistribution data normalized to organ mass, normalized to total radiant efficiency over all organs (c). Blood circulation profiles of nanoparticles, evaluated by measuring blood samples on the IVIS. (d). Retention of NPs at 3h, as a percentage of the amount measured at $t = 0$. For 8a, 8b, and 8c, $n = 3$ and for 8d $n = 6$; for all experiments, ns: $p > 0.05$; *: $p \leq 0.05$; **: $p \leq 0.01$; ***: $p \leq 0.001$ as determined through 2-way ANOVA with Bonferroni post-tests.
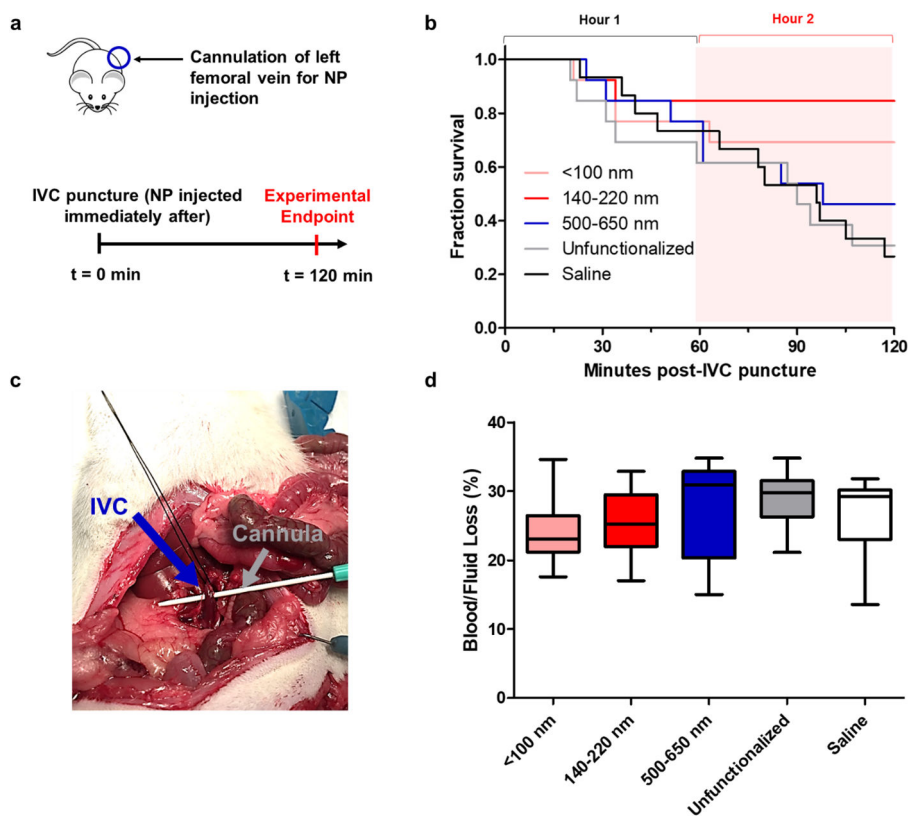
Figure 9. Hemostatic efficacy of three different sized nanoparticles in a lethal inferior vena cava puncture model in Sprague-Dawley rats.

(a). Dosing schedule and surgical procedure; (b) Kaplan-Meier survival curves of hemostatic nanoparticles (pink, red, blue, n = 13 each), unfunctionalized nanoparticle (gray, n = 13), and saline (black, n = 15). (c) Image of puncture through IVC with cannula; (d). Blood /fluid loss as measured by pre-weighed gauze.
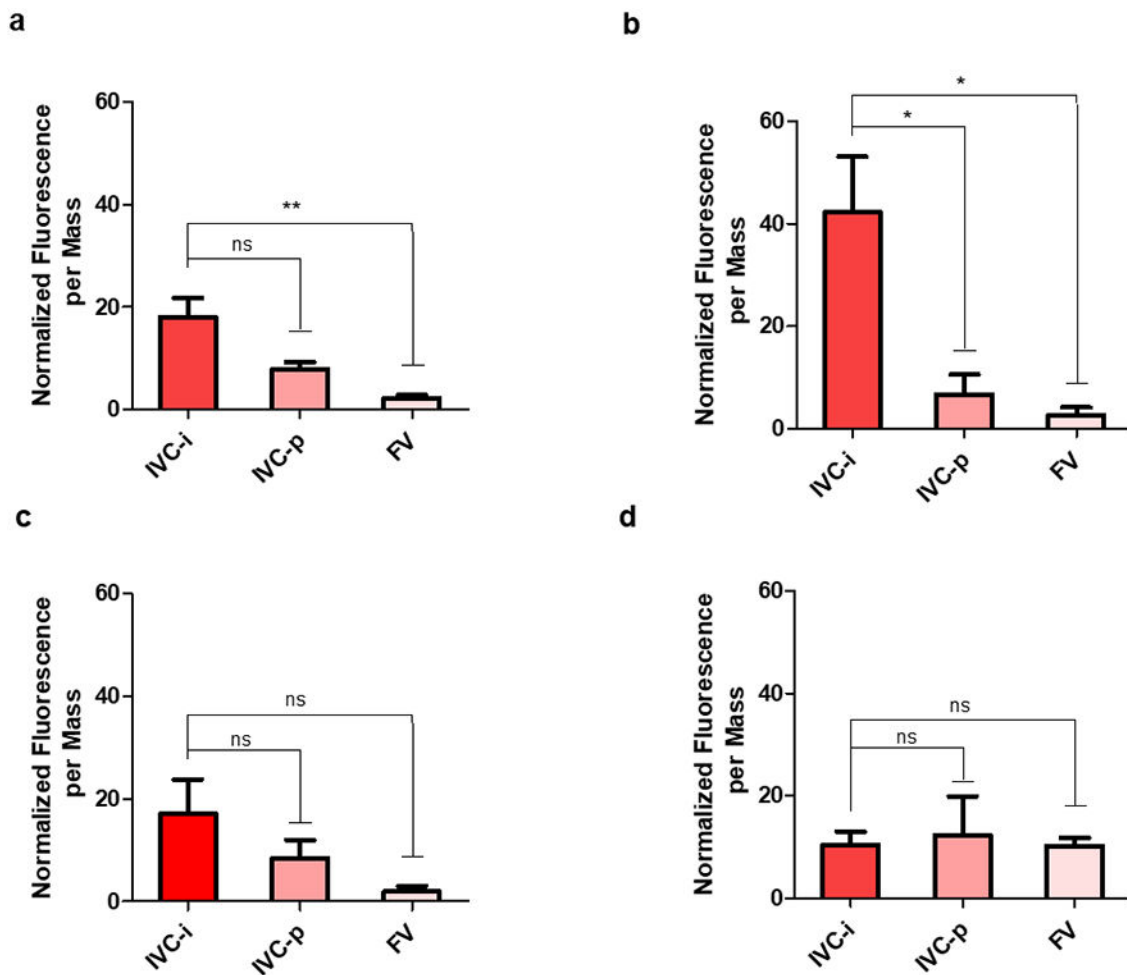
Figure 10. Accumulation of Cy7-labeled nanoparticles in vessel segments.
(a). Small (<100 nm) nanoparticles. (b) Intermediate (140-220 nm). (c) Large (500-650 nm) nanoparticles. (d) Unfunctionalized (140-220 nm) nanoparticles. The injured IVC, uninjured (proximal) IVC, and uninjured femoral vein are denoted as (IVC-i, IVC-p, and FV, respectively). For all experiments, n = 3, and ns: $p > 0.05$; *: $p \le 0.05$; **: $p \le 0.01$; ***: $p \le 0.001$ as determined through one-way ANOVA with Bonferroni post-tests.
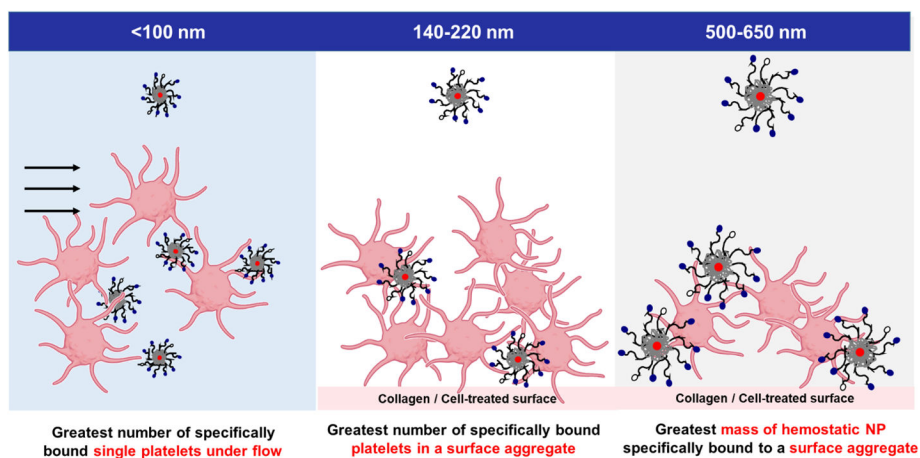
Scheme 1: Summary of *in vitro* experimental results for particle sizes to be tested in the lethal injury model.

Sub-100 nm nanoparticles resulted in the greatest number of specifically bound platelets under flow; intermediate-sized nanoparticles resulted in the greatest number of platelets in a platelet-particle surface aggregate, and largest particles resulted in the greatest polymer mass accumulation onto platelet-particle surface aggregates. Adapted from Biorender [39].

Table 1.

Sample synthesis conditions for nanoparticles of various sizes

Desired Size (nm)	Solvent	Polymer Conc.	PEG-PLGA/ PLGA ratio	Synthesis Method
<100	DMF	5 mg/mL	5:1	Nanoprecipitation
110-130	DMF	10 mg/mL	5:1	Nanoprecipitation
140-220	THF[*]	20 mg/mL	5:1	Nanoprecipitation
250-400	Acetonitrile[*]	100 mg/mL	5:1	Nanoprecipitation
500-650	DMSO	8 mg/mL	5:1	Dialysis

[*] For batch 2, sizes 140-220 nm and 250-400 nm were synthesized using 15 mg/ mL,50:50 DMF: THF (volume ratio) and 20 mg/ mL THF, respectively.

Table 2.

Kaplan-Meier analysis (Logrank / Mantel-Cox Test) of nanoparticle sizes and controls

	Full two-hour experiment		Hour 1-Hour 2	
	P-Value	Significance[*]	P-Value	Significance[*]
140-220 nm VS Saline	0.006	**	0.0015	**
140-220nm VS UF (same size)	0.0089	**	0.0087	**
140-220 nm VS 500-650 nm	0.0585	ns	0.0415	*
140-220 nm VS<100 nm	0.3707	ns	0.2943	ns
<100 nm VS saline	0.081	ns	0.0209	*
<100 VS 500-650 nm	0.3224	ns	0.2385	ns
500-650 nm VS saline	0.4437	ns	0.2438	ns

[*]
Significance: ns: p > 0.05

[*]
: p   0.05

[**]
: p   0.01.